Cell Reports

Article

Antennapedia and *optix* regulate metallic silver wing scale development and cell shape in *Bicyclus anynana* butterflies

Graphical abstract

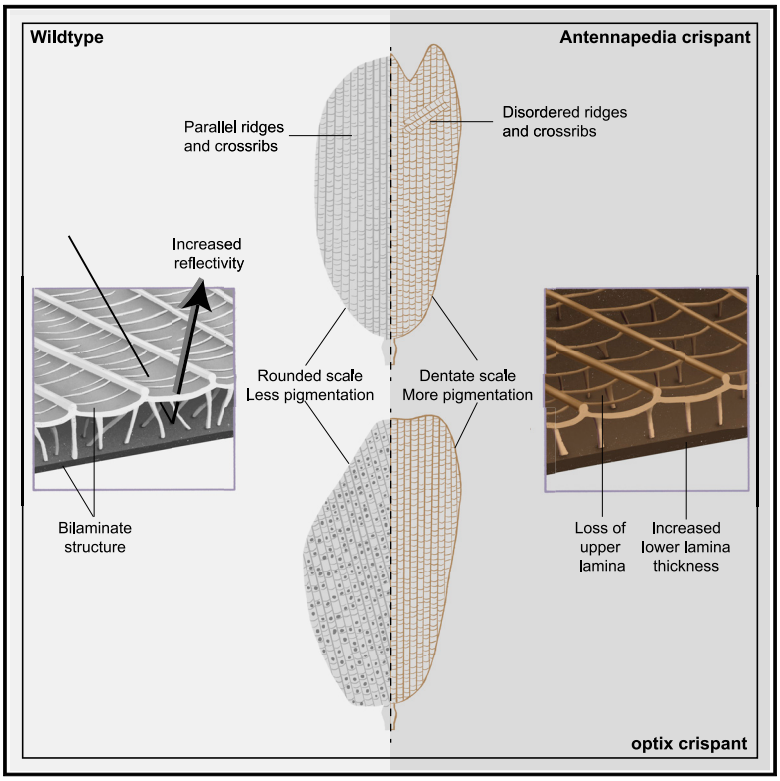

Highlights

- Bilaminate scale structure increases silver reflectivity compared with a single lamina
- Varying air gap layer is the key scale parameter to produce broadband silver colors
- *Antennapedia* and *optix* determine cell shape, structure, and color in silver scales
- *Antennapedia* regulates ridge and crossrib orientation in wing scales

Authors

Anupama Prakash, Cédric Finet, Tirtha Das Banerjee, Vinodkumar Saranathan, Antónia Monteiro

Correspondence

anupama@u.nus.edu (A.P.), antonia.monteiro@nus.edu.sg (A.M.)

In brief

Silvery structural colors in butterfly wing scales are predominantly produced by bilaminate nanostructures with a sandwiched air layer, but their genetic and optical basis are unclear. Prakash et al. show that a bilaminate structure increases silver reflectivity and identify *Antennapedia* and *optix* as regulators of pigmentation, ultrastructure, and scale shape.

Prakash et al., 2022, Cell Reports *40*, 111052
July 5, 2022
https://doi.org/10.1016/j.celrep.2022.111052

CellPress

Cell Reports

CellPress
OPEN ACCESS

Article

Antennapedia and *optix* regulate metallic silver wing scale development and cell shape in *Bicyclus anynana* butterflies

Anupama Prakash,[1,*] Cédric Finet,[2] Tirtha Das Banerjee,[1] Vinodkumar Saranathan,[1,2,3] and Antónia Monteiro[1,2,4,*]
[1]Department of Biological Sciences, National University of Singapore, Singapore, Singapore
[2]Division of Science, Yale-NUS College, National University of Singapore, Singapore, Singapore
[3]Present address: Division of Sciences, School of Interwoven Arts and Sciences, Krea University, Sricity, India
[4]Lead contact
*Correspondence: anupama@u.nus.edu (A.P.), antonia.monteiro@nus.edu.sg (A.M.)
https://doi.org/10.1016/j.celrep.2022.111052

SUMMARY

Butterfly wing scales can develop intricate cuticular nanostructures that produce silver colors, but the underlying genetic and physical basis of such colors is mostly unexplored. Here, we characterize different types of wild-type silver scales in *Bicyclus anynana* butterflies and show that the varying thickness of the air layer between two cuticular laminas is most important for producing silvery broadband reflectance. We then address the function of five genes—*apterous A*, *Ultrabithorax*, *doublesex*, *Antennapedia*, and *optix*—in silver scale development by examining crispants with either ectopic gains or losses of silver scales. Simultaneous transformations of three parameters—loss of the upper lamina, increased lower lamina thickness, and increased pigmentation—occur when silver scales become brown and vice versa when brown scales become silver. *Antennapedia* and *optix* are high-level regulators of different silver scale types and determine cell shape in both sexes. Moreover, *Antennapedia* is involved in determining ridge and crossrib orientation.

INTRODUCTION

Silver or gold colors in insect cuticles (Land, 1972; Neville, 1977; Seago et al., 2009), fish scales (Denton and Land, 1971), and the eyes of cephalopods (Denton and Land, 1971; Gur et al., 2018; Holt et al., 2011; Land, 1972) are all examples of naturally occurring broadband structural coloration. These colors serve multiple ecological functions including in vision, as inter- or intra-specific signals, or in thermoregulation (Denton, 1970; Holt et al., 2011; Johnsen, 2014; Nan et al., 2015; Stavenga et al., 2015; Wagner et al., 2009; Wilts et al., 2013) and arise from the interaction of light with specific classes of broadband reflectors found in the animal integument (Kinoshita et al., 2008; Srinivasarao, 1999; Vukusic and Sambles, 2003).

Broadband metallic reflectors, which are highly reflective across a broad range of wavelengths, usually involve thin film or multilayer interference made of alternating materials with different refractive indices and varying thicknesses (Land, 1972; Parker et al., 1998). Examples of such multilayer broadband reflectors are found in the exocuticle of gold beetles (Finlayson et al., 2017; Parker et al., 1998), the endocuticle of some butterfly pupal cases (Neville, 1977; Steinbrecht, 1985; Steinbrecht et al., 1985), and in fish scales (Gur et al., 2018; McKenzie et al., 1995). Due to the small difference in refractive indices of biological materials, broadband multilayer reflectors with high reflectivity usually require a minimum of 10–20 alternating layers of high- and low-refractive index materials, leading to very thick (tens of microns) multilayer reflectors (Steinbrecht et al., 1985).

In contrast, broadband metallic reflectors found in lepidopteran wing scales are anatomically constrained by the thickness of the scales. These metallic reflectors are ultra-thin, with an overall thickness of a few microns (D'Alba et al., 2019; Kilchoer et al., 2019; Ren et al., 2020; Vukusic et al., 2009; Wilts et al., 2013). An essential modification of the basic scale Bauplan to produce such broadband reflectors is the consistent presence of a contiguous upper lamina that closes the normally "open" windows seen in a typical scale (Ren et al., 2020; Simonsen, 2007; Vukusic et al., 2009; Wilts et al., 2013). This creates an undulatory air layer sandwiched by the lower and upper laminas whose thicknesses also vary spatially. Broadband reflectance is achieved by additive color mixing that occurs due to local spatial variation or disorder in the scale ultrastructure (D'Alba et al., 2019; Dolinko et al., 2021; Ren et al., 2020; Vukusic et al., 2009; Wilts et al., 2013). This means that a single silver scale, when observed at very high resolution, is made up of many small patches of distinct colors, such as blues, greens, oranges, and pinks. The broadband metallic reflectors seen in fossil moths (D'Alba et al., 2019; Qingqing et al., 2021), in extant moths (Kilchoer et al., 2019), and in springtails (Vanthournout et al., 2021), however, utilize thin-film interference from a single chitin layer, resulting from fused scales. Such a single thin film is also present as the lower lamina of archetypal butterfly scales, which are often also tuned to produce broadband colors (Thayer

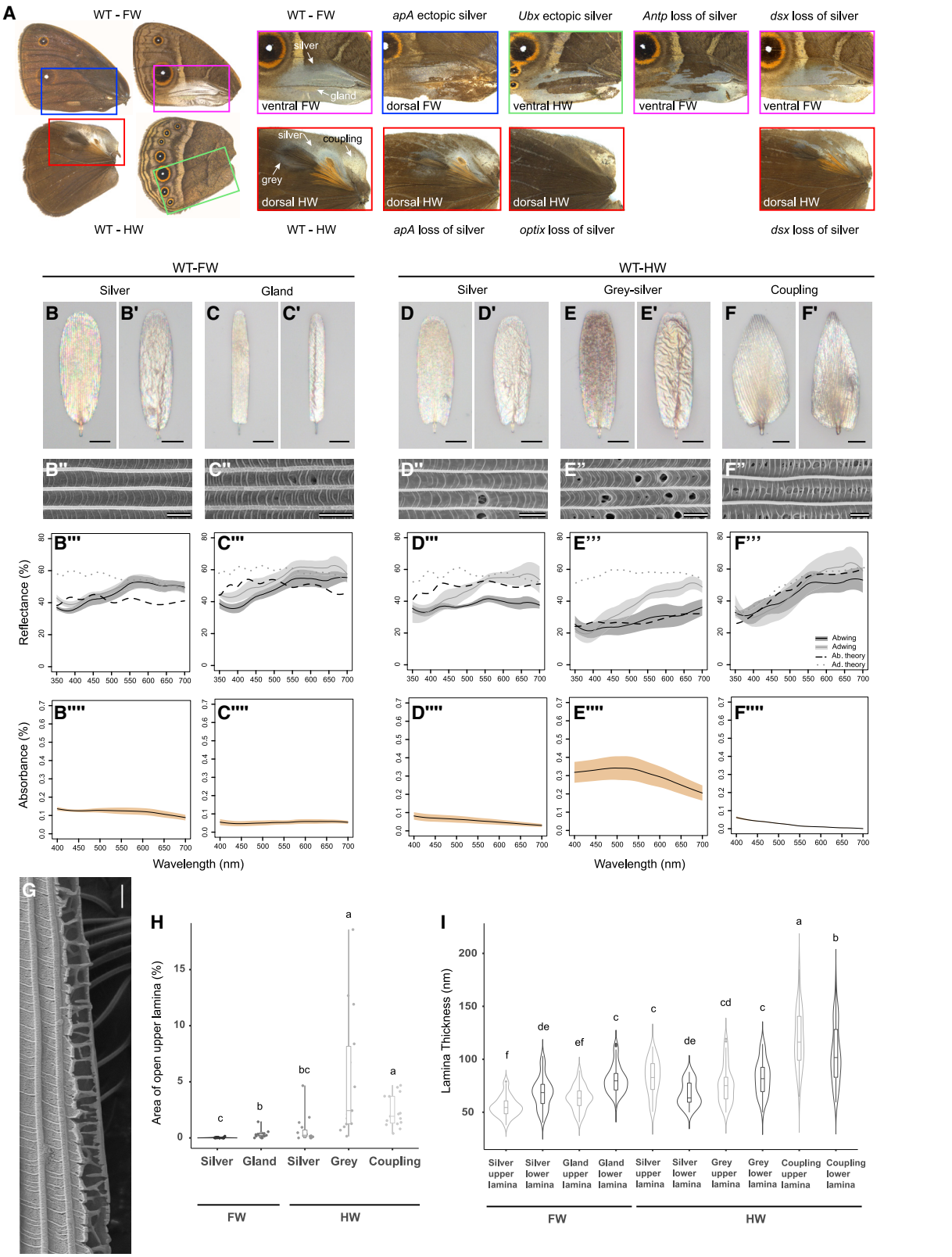

(legend on next page)

et al., 2020; Wasik et al., 2014). Therefore, the necessity and advantage(s) of a bilaminate system in broadband scale color generation, a trait that has repeatedly evolved across butterflies, is enigmatic.

The production of metallic broadband reflectors may also depend on the absence of pigments embedded in the scale cuticle. For instance, the brown ground scales in *Hypolimnas salmacis*, the yellow scales in *Heliconius* butterflies, and the "black" scales in the *yellow* mutant of *Bicyclus anynana* butterflies have a closed upper lamina (Livraghi et al., 2021; Matsuoka and Monteiro, 2018; Siddique et al., 2016), but these scales do not exhibit broadband reflectance due to either the high concentration of pigments or incorrect thicknesses of both the laminas and air layer in these scales. These examples suggest that the regulatory networks that create a metallic scale type must involve regulation of scale ultrastructure dimensions, perhaps along with pigmentation. Although the optical origin of broadband silvery colors from thin-film and chirped multilayer reflectors in the arthropod integument is well understood (D'Alba et al., 2019; Dolinko et al., 2021; Neville, 1977; Steinbrecht et al., 1985; Vukusic et al., 2009; Wilts et al., 2013), the necessity of a bilaminate air-filled nanostructure, the relative contributions of air gap layer versus upper and lower laminas, and the genetic circuits that create these broadband metallic reflectors in butterfly wing scales remain unclear despite a number of studies on silvery butterfly scales (Dolinko et al., 2021; Ren et al., 2020; Vukusic et al., 2009; Wilts et al., 2013).

We have begun to explore the genetic basis of silver scale development with a series of CRISPR experiments performed in the nymphalid butterfly *B. anynana*. This species exhibits different types of broadband reflecting metallic scales on both fore- and hindwings (Prakash and Monteiro, 2020). These scales are usually associated with the sex pheromone producing regions in males (the androconia), except for the coupling scales near the base of the wings that are present in both sexes. Previously, the knockout of four genes, including *apterous A* (*apA*) (Prakash and Monteiro, 2018), *Ultrabithorax* (*Ubx*) (Matsuoka and Monteiro, 2021), *doublesex* (*dsx*) (Prakash and Monteiro, 2020), and *Antennapedia* (*Antp*) (Matsuoka and Monteiro, 2021) led to both gains and losses of silver scales in *B. anynana* (Figure 1A). In addition, we speculated that *optix* might be a good candidate regulating metallic coupling scale development in *B. anynana*, given the expression and function of this gene in the development of coupling scales in other butterflies (Martin et al., 2014; Zhang et al., 2017). All modified scales provided an opportunity to investigate the structural basis of the different silver colors and to understand the roles of these genes in creating broadband reflectors in lepidopterans.

Among the genes investigated, *apA* and *Ubx* are well known homeotic genes that specify wing-surface or wing-specific identities in butterflies, respectively (Matsuoka and Monteiro, 2021; Prakash and Monteiro, 2018; Tendolkar et al., 2021; Weatherbee et al., 1999). In *B. anynana*, *apA* expression is restricted to dorsal wing surfaces and *Ubx* is restricted to hindwings, and both genes have homogeneous expression across those wings/surfaces (Matsuoka and Monteiro, 2021; Prakash and Monteiro, 2018). In contrast, *Antp* and *dsxM* show strong punctate expression within individual scale cells in a trait-specific manner, including in eyespot centers, pheromone glands, and the silver scale regions (Matsuoka and Monteiro, 2021; Prakash and Monteiro, 2020), hinting at a functional role of these two genes in differentiating specific scale types. Here, we asked whether the investigated genes modified different structural and pigmentary aspects and components of the scale to create a silver color and vice versa when silver scales became brown. We examined whether transformations of different structures and levels of pigmentation within a scale, with the manipulation of each gene in isolation, was partial or complete. We hypothesized that the two homeotic genes would produce more complete and extreme transformations of the scales, making them resemble a wild-type (WT) silver scale (or a brown scale) more closely while the trait-specific genes would have more restrictive transformations, affecting only aspects of either color or morphology.

To answer these questions, we first examined the potential role of *optix* in the development of silver-colored coupling scales in *B. anynana* by use of immunostainings and CRISPR, and we identified that *optix* is necessary for coupling scale development. We then used light, conventional, and focused ion beam (FIB) scanning electron microscopy (SEM), UV-VIS-NIR microspectrophotometry, and systematic optical modeling, to understand different aspects of the WT and transformed scales for all five genes. We show that the bilaminate structure of metallic scales increases broadband reflectivity in contrast to a single thin film and that the variable air layer thickness in silver scales is the most important determinant of the broadband nature of the reflectance. Transformation of silver to brown scales is accompanied by loss of the contiguous upper lamina, increase in lower lamina thickness and gain in pigmentation. The opposite occurs when brown scales become silver scales. In addition, we identify *Antp* and *optix* as high-level regulators of the different silver scale types, determining both scale shape and scale color via modulation of ultrastructure dimensions.

Figure 1. *B. anynana* crispants sampled in this study and broadband reflectors in WT *B. anynana*

(A–F‴) (A) WT dorsal and ventral wing surfaces with magnified views of the silver scale regions alongside ectopic silver scales or silver-to-brown transformed scales in crispants of the five genes. The colored box outlines and the text label in each inset indicate the position on the different wing surfaces of the WT and crispant scales. White arrows in the WT panels indicate the five different silver scale types characterized. Optical microscopy images of the abwing (upperside) (B–F) and adwing (underside) (B′-F′) surfaces of single scales, SEM images of the abwing surface (B″–F′), measured and modeled reflectance (B‴–F‴) and absorbance spectra (B⁗–F⁗) of the WT forewing silver and gland scales and the hindwing silver, gray-silver and coupling scales respectively.

(G) A longitudinal cross-section of a forewing silver scale showing the upper and lower laminas enclosing an air layer.

(H) Area of the open upper lamina of the different silver scales on the forewings and hindwings. Boxplots show the median, inner, and outer quartiles and whiskers up to 1.5 times the inter-quartile range.

(I) Violin plots of the upper and lower lamina thicknesses of the different forewing and hindwing silver scales. Means sharing the same letter are not significantly different (Tukey-adjusted comparisons). Scale bars: (B), (B′–F), and (F′) are 20 μm; (B″–F′) and (G) are 2 μm.

RESULTS

optix is required for the development of silver colored, trowel-shaped coupling scales in *Bicyclus anynana*

We first investigated the role of *optix* in coupling scale development using immunostainings and CRISPR-Cas9 gene knockouts. Optix protein was highly expressed in punctate nuclei of the future coupling scales on the developing pupal dorsal hindwings at all three time points investigated (Figures S1A–S1D). Mosaic crispants that resulted from embryonic injections of two guide RNAs against *optix* revealed a silver-to-brown color transformation of the coupling scales along with a change in shape from typical trowel-shaped scales to scales with rounded or slightly scalloped distal edges (Figures S1E–S1J). These results indicate that, like *Antp* and *dsx* (Matsuoka and Monteiro, 2021; Prakash and Monteiro, 2020), *optix* is expressed in a trait-specific manner and is required for regulating the color and shape of the silver coupling scales in *B*. *anynana*.

Ultrastructural and optical origin of broadband silver reflections in *B*. *anynana* butterflies

We then investigated how the silver color is produced in five types of silver scales present on the wings of *B*. *anynana* by using light reflection and absorbance measures, as well as SEM (Figures 1B–1G). On the ventral forewing (FW), we focused on the silver and the gland scales on the androconial patch of males (Figure 1A, WT-FW arrows). On the dorsal hindwing (HW), we sampled the silver and gray-silver scales near the androconial patches of males. Finally, we sampled coupling scales near the base of the dorsal hindwing in females (Figure 1A, WT-HW arrows). All silver scales generally feature rounded edges. The coupling scales, however, have a characteristic trowel-head shape (Figures 1F and 1F′), and their ridges are oriented at an angle to the proximodistal axis of the scale compared with the parallel arrangement of ridges in most other scale types. The abwing (upperside) and adwing (underside) surfaces of the scales exhibited an oil-slick-like multi-hued appearance, typical of a thin film with varying thickness (Figures 1B–1F). The reflectance spectra of all silver scales exhibited broadband (relatively flat or uniform) reflectance, with higher intensities from the adwing surface (Figures 1B‴–1F‴). Pigmentation levels were low in all scales, as measured from low light absorbance (Figures 1B⁗–1F⁗), with the exception of the gray-silver scales, which absorbed more light, indicating higher levels of pigmentation. All silver scales exhibited a closed upper lamina (Figures 1B″–1F″), creating a bilaminate structure enclosing an air layer (Figure 1G). The different silver scale types exhibited varying levels of perforations in the total area of upper lamina (Figure 1H and Table S5, source data): from ~0% (fore- and hindwing silver scales) and 2.35% (hindwing coupling scales) to 5.4% open (hindwing gray-silver scales) (Tables S1 and S2). This correlation between the integrity of the upper lamina coverage to the production of broadband reflectance affirms the important role attributed to the upper lamina and/or the enclosed air layer.

In order to theoretically model these broadband metallic colors, we measured the air gap and lower, and upper lamina thicknesses from FIB-SEM cross-sections of the different silver scale types (Figures 1G and 1I and Table S5, source data). The mean upper and lower lamina thicknesses of the different metallic scale types ranged from approximately 55 to 120 nm, with the coupling scales having the thickest lower and upper laminas (Figure 1I). We modeled the theoretical adwing and abwing spectra, the latter by incorporating the measured absorptivity curves (Figures 1B⁗–1F⁗), which produced broadband reflectance with a series of very shallow peaks and whose positions are largely consistent with those in the corresponding measured spectra (Figures 1B‴–1F‴, and S2). A lower lamina thin film of an appropriate thickness could, alone, produce a broadband silver color (Figure S3A). However, our results indicated that the presence of the additional upper lamina enclosing an air gap with varying thickness increased the mean broadband reflectivity by around 11% (Figure S3A). Furthermore, our hierarchical modeling (Figures S3 and S4) suggests that the varying air gap layer is the most important component of the bilaminate three-layer nanostructure responsible for a broadband silvery reflectance. For instance, the simulated patches with distinct colors (e.g., purple-pink and blue-green; Figure S3C) not only correspond well to those seen in the high-magnification light micrographs (Figures 1B, 1B', and S3C) but also combine to make a broadband color in the far-field in a Pointillist fashion (Ren et al., 2020). However, changing the upper and/or lower lamina thicknesses with a constant air gap thickness cannot reproduce the relatively flat broadband reflectance, even when accounting for the increased lamina thicknesses (i.e., greater variability) at or near the ridges (cf. Figures S3A and S3D).

Interestingly, our systematic parametric modeling (Figure S4) revealed that the thicknesses of both upper and lower laminas for each of the silver scale types, except for the coupling scales, are optimized to produce the maximum broadband reflectivity. By contrast, the air gap layer is sufficiently thick (>750 nm) to ensure the broadband nature of the reflectivity. A thickness of less than 500 nm would produce strong peak(s) with chromatic effects destroying the silvery appearance (Figure S4). The modeling results also predicted lower reflectivity at short wavelengths below 450 nm for the coupling scales (Figure S4N), like their measured spectra (Figure 1F″). Given that the coupling scales are among the least pigmented of the silver scales (Figure 1F⁗), our results indicate that this lower reflectivity is a previously undocumented structural rather than a pigmentary effect. The lower reflectivity is caused by a decrease in the thickness of the lower lamina from base to tip (Figure S5) that results in a concomitant change in the color of the scale from bronze/brown in the base/center to silver at the tips. The increased thickness near the base of the scale suppresses shorter wavelengths of light and leads to a grayish darker color (Figure 1F′), whereas optimum thickness toward the tip reinforces broadband silver reflectance.

Antp regulates silver scale shape and color, but *dsxM* regulates only scale color

Both *Antp* and *dsx* male crispants exhibited a silver to brown color transformation on the forewing but had different effects on scale shape (Figures 2A–2C). The rounded edges of the distal end of the silver scales of *Antp* crispants changed into serrated finger-like projections, resembling other brown scales on the same wing surface (Figures 2D and S6A). This was also true in

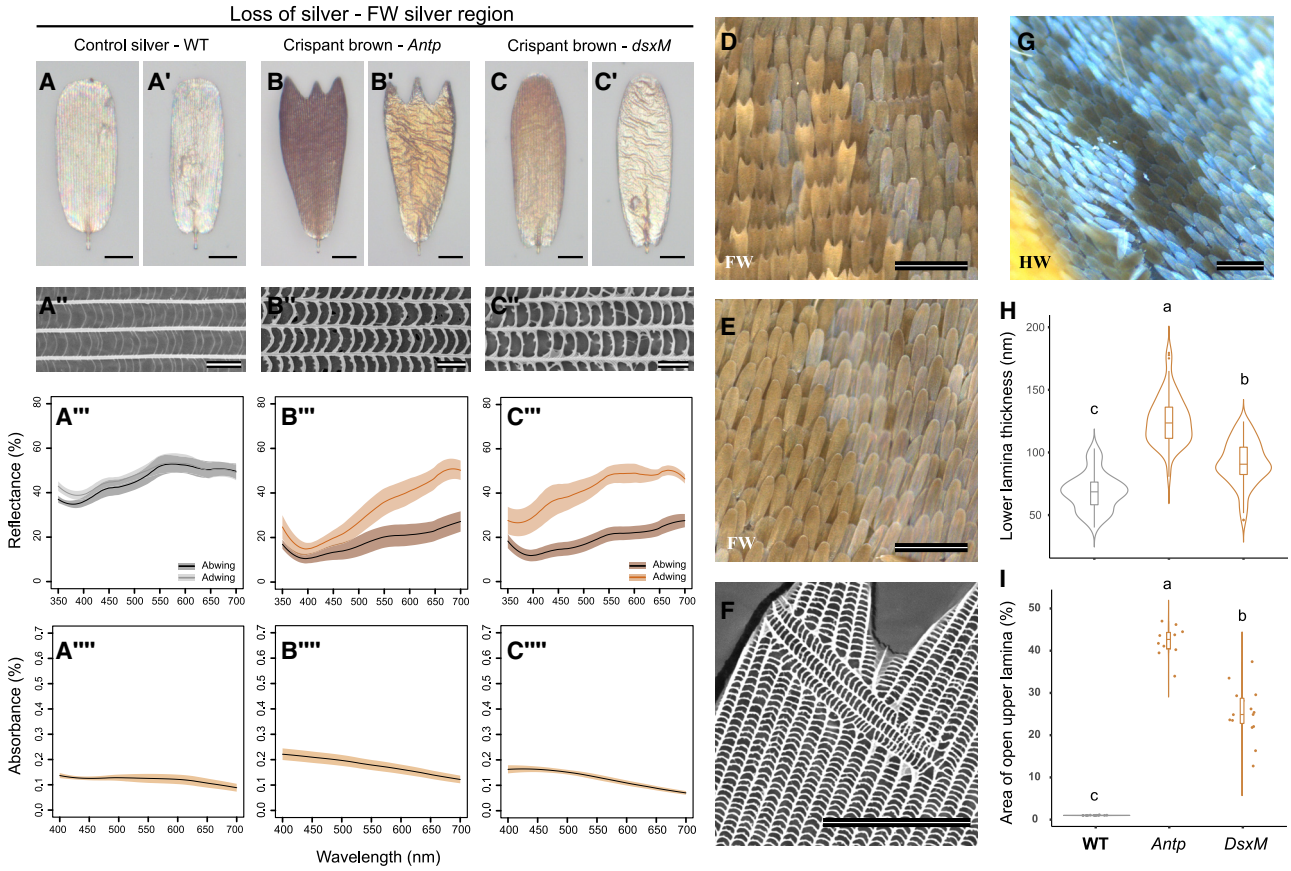

Figure 2. Characterization of the ultrastructure and pigmentation of the silver to brown scales in *Antp* and *dsxM B. anynana* crispants

(A–C) Optical microscopy images of the abwing (A–C) and adwing (A′–C′) surfaces, SEM images of the abwing surface (A″–C″), reflectance (A‴–C‴) and absorbance spectra (A⁗–C⁗) of the WT forewing control silver scales and the mutant brown scales of *Antp* and *dsxM* crispants, respectively.

(D) Mosaic scale phenotype in *Antp* crispant forewing (FW) illustrating the mutant brown scales with dentate sculpting in the distal tips.

(E) Mosaic scale phenotype in *dsxM* crispant forewing (FW) illustrating the mutant brown scales with rounded distal tips.

(F) SEM image of an *Antp* crispant forewing brown scale showing a nearly orthogonal ridge and crossrib orientation among the normal ridges and crossribs. These variations always occur at the distal tips of the crispant scales (N = 4 scales from one individual).

(G) Mosaic scale phenotype in male *Antp* crispant hindwing (HW) illustrating the mutant brown scales with dentate sculpting in the distal tips.

(H and I) Violin plots of the lower lamina thicknesses of the control silver scales and the crispant brown scales of *Antp* and *dsxM* crispants (I) Total area of open upper lamina of the different control and mutant scales. Boxplots show the median, inner, and outer quartiles and whiskers up to 1.5 times the inter-quartile range. Means sharing a letter are not significantly different (Tukey-adjusted comparisons). Scale bars: (A, (A′–C), (C′), and (F) are 20 μm; (A″–C′) are 2 μm; (D), (E), and (G) are 200 μm.

Antp crispant females, where the normal rounded brown scales on the posterior region of the ventral forewings became brown scales with dentate margins in the crispants (Figure S6B). Furthermore, some of the *Antp* crispant brown scales exhibited unusual ridge and crossrib orientations near the distal tips of the scales, often lying perpendicular to the normal parallel arrangement of ridges (Figures 2F and S6E). In contrast, the loss of *dsxM* expression in the same region in males produced brown scales with a rounded distal edge (Figure 2E). Loss of *dsxF* in females had no effects on scale color or shape in the homologous regions (Prakash and Monteiro, 2020). On the hindwing silver areas, we noticed similar small clonal patches of brown scales in *Antp* male crispants (Figure 2G). Such clonal patches were also visible on female hindwings of *Antp* crispants in homologous regions of the wing, though not as contrasting (Figure S6D). The brown scales in these clonal patches had a dentate morphology like other dorsal hindwing scales, in contrast to the rounded scales seen in the hindwing silver scale region in males or the homologous regions in females (Figures S6C and S6D).

Ultrastructure and pigmentation modifications accompanied the loss of silver reflectance in male scales of both crispant types. The brown crispant scales had lower reflectivity compared with the WT control scales (Figures 2A‴–2C‴), and this was accompanied by an increase in absorbance due to greater pigmentation (Figures 2A⁗–2C⁗). The crispant brown scales also lost their continuous upper lamina, which now exhibited perforated windows (Figures 2A″–2C″ and 2I, Tables S1 and S2). Other ultrastructural modifications included an increase in lower lamina thickness (Figure 2H) (post hoc tests from LME,

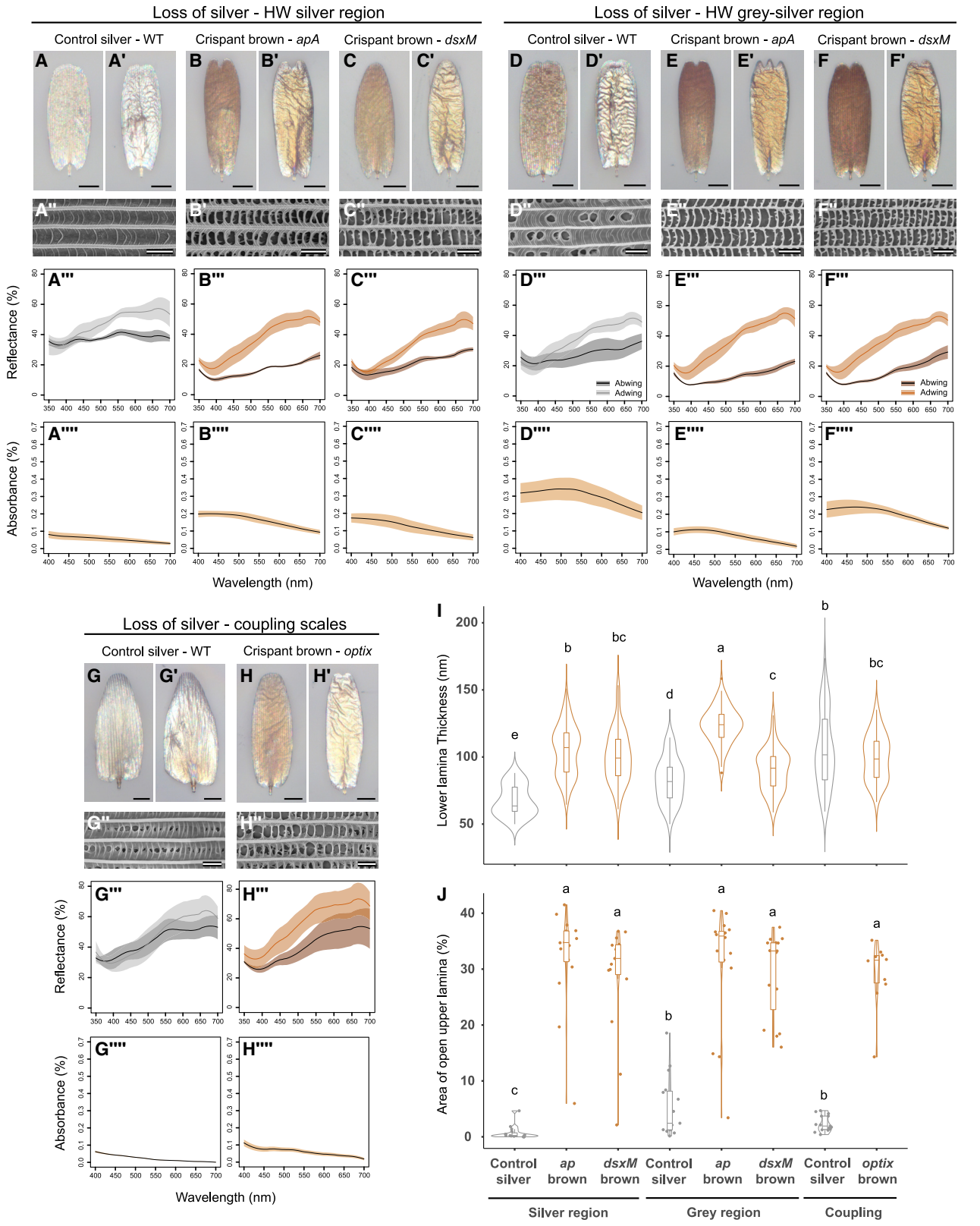

(legend on next page)

adjusted p values <0.001; Tables S3 and S4). *Antp* brown scales had a greater lower lamina thickness (125.82 ± 19.7 nm) compared with the *dsxM* brown scales (91.9 ± 17.6 nm), and both were significantly different from WT silver lower lamina thickness (68.8 ± 14.75 nm). The increase in pigmentation, loss of the upper lamina, and increased lower lamina thickness led to the loss of broadband metallic silver reflectance and created a brown color due to the combination of pigments and the now dominant lower lamina reflectance (Figures 2A‴–2C‴).

These results suggest that *Antp* is an important high-level regulator in the silver scale differentiation program and is necessary to determine correct silver scale color and morphology in males and scale shape in females. *Antp* likely acts upstream of, or in parallel with, *dsxM*, which appears to have similar effects on color and upper lamina morphology but does not impact scale shape. In addition, *Antp* crispant scales showed larger changes in lower lamina thickness and area of open upper lamina compared with *dsxM* crispant scales (Figures 2H and 2I). To investigate the extent to which Antp expression maps to silver scales, we examined the expression of Antp in 24-h male and female pupal wings. Antp protein was visible in punctate nuclei in the forewing (Figure S7A) and hindwing silver scale regions in males, especially around the future hindwing gland (Figure S7C), and also in female wings at homologous locations (Figures S7B and S7D). Antp protein expression was lower in the gray-silver scales on male hindwings (Figure S7C). This pattern on male hindwings was especially clear in a 48-h pupal hindwing (Figure S8). These data indicate that Antp protein maps precisely to punctate nuclei in the area where silver scales develop on both wings, as expected of a transcription factor.

apA, *dsxM*, and *optix* promote silver coloration via the gain of an upper lamina, a decrease in lower lamina thickness, and a loss of pigmentation

On the hindwings, crispants of *apA*, *dsx*, and *optix* showed loss of metallic silver scales and transformation of these scales into brown scales. For *apA*, these are the exact opposite phenotypes from those observed on the forewing, where *apA* transformed brown scales into ectopic silver scales. In *apA* and *dsxM* crispants, hindwing silver and gray-silver scales were transformed into brown scales (Figures 3A–3F). Brown crispant scales of *apA* individuals exhibited a dentate morphology, whereas those in *dsxM* individuals exhibited some variation in morphology, from rounded scales in the silver region to sometimes dentate scales in the gray-silver region. Crispants of *optix* affected both the shape and the color of coupling scales (Figures 3G, 3H, and S1H–S1J). Reflectance spectra reflected the change in coloration (Figures 3A‴–3H‴). In all instances of transformation, the adwing sides of the crispant scales were thin films reflecting a deep bronze-golden color instead of the silver-to-gold reflectance of the WT control scales (Figures 3A'–3H'). In addition, in line with the silver to brown transformation, there was an increase in pigmentation in most scales (Figures 3A⁗–3C⁗ and 3G⁗–3H⁗), except in the gray-silver region, where crispant brown scales, in both *apA* and *dsxM* crispants, had decreased pigmentation compared with the controls (Figures 3D⁗–3F⁗) despite control scales displaying a lot of variation in pigmentation levels (Figure 3D⁗).

Crispant brown scales on the hindwing, produced by all three genes, also exhibited a loss of the upper lamina (Figures 3A″–3H″ and 3J, Tables S1 and S2). This was not a clean morphological change, with many scales exhibiting a gradualism in transformation, often having remnants of the lamina attached to the cross-ribs and ridges (Figures 3A″–3H″, and 3J). The lower lamina thickness of these scales also increased compared with WT silver controls (post hoc tests from LME, adjusted p values <0.001; Tables S3 and S4). Both *apA* and *dsxM* hindwing brown scales in the silver and gray-silver regions had significantly thicker lower laminas than control scales, whereas there was no change of lamina thickness in *optix* crispant brown scales (Figure 3I, Tables S3 and S4).

Ectopic silver scales gain an upper lamina, have a thinner lower lamina, and lose pigmentation

We next investigated the ectopic forewing silver scales produced in the *apA* and *Ubx* crispants by the transformation of non-reflective brown scales (Figure 1A). We characterized both ectopic silver and gland scale types in *apA* crispants but only the ectopic silver scale type in the single *Ubx* crispant due to size limitation of the mutant clone in that individual. Ectopic silver scales in both *apA* and *Ubx* crispants looked like WT silver scales, including changes in cell shape (Figure 4). The *Ubx* crispant scales exhibited an extensive transformation, from scalloped brown scales to rounded silvery scales (Figures 4D and 4E), whereas the *apA* crispant scales changed primarily in color and less extensively in shape (Figures 4A–4C). The abwing and adwing surfaces of the ectopic scales were metallic silvery thin films (Figures 4B, 4C, and 4E). These scales were dramatically different from the control brown scales from the same crispant regions, which were brown in color from the abwing side (Figures 4A and 4D) and had a bronze-golden adwing thin film (Figures 4A′ and 4D'). Reflectance spectra corresponded to the optical images, with the silver scales reflecting broadly (Figures 4A⁗–4E⁗). Ectopic metallic scales of both *apA* and *Ubx* crispants also lost pigmentation compared with the control brown scales, although there was variation between the different scale types (Figures 4A⁗–4E⁗).

Structural modifications accompanying brown-to-silver scale transformations, in *apA* and *Ubx* crispants, were

Figure 3. Characterization of the ultrastructure and pigmentation of transformed silver to brown scales in *apA*, *dsxM*, and *optix B. anynana* crispants

(A⁗–H⁗) Optical microscopy images of the abwing (A–H) and adwing (A′-H′) surfaces, SEM images of the abwing surface (A″–H″), reflectance (A‴–H‴), and absorbance spectra (A⁗–H⁗) of the control WT silver scales and transformed crispant brown scales in the hindwing silver region (A–H), the hindwing gray-silver region (D–F), and the hindwing coupling scales (G and H). The control scales are WT silver scales from homologous regions on the wing.

(I–J) Violin plots of the lower lamina thicknesses of control WT silver scales and the crispant brown scales of *apA*, *dsxM*, and *optix* crispants. (J) Total area of open upper lamina of the different control and crispant brown scales. Boxplots show the median, inner, and outer quartiles and whiskers up to 1.5 times the interquartile range. Means sharing a letter are not significantly different (Tukey-adjusted comparisons). Scale bars: (A), (A′–H), and (H') are 20 μm; A″–H″ are 2 μm.

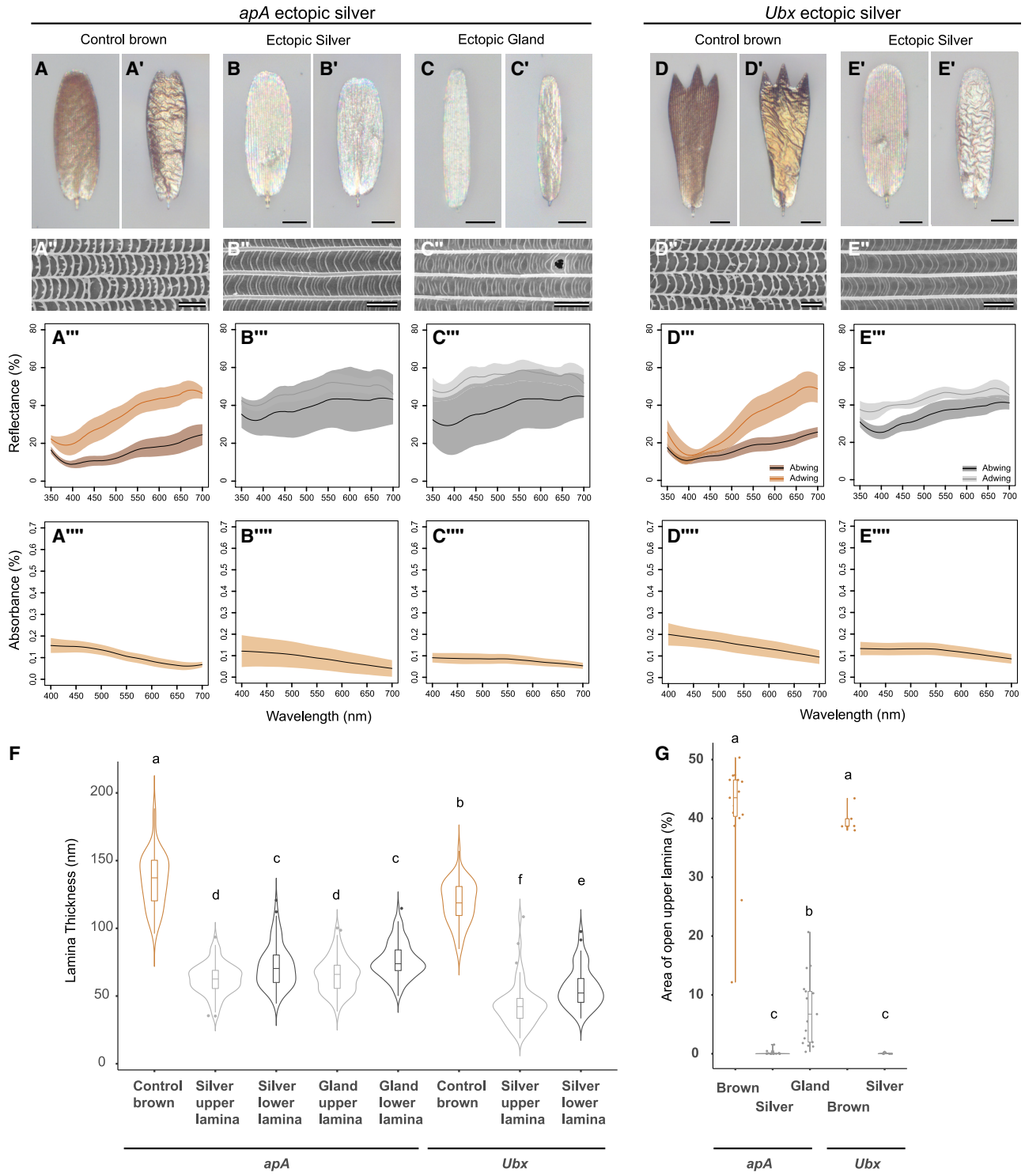

Figure 4. Characterization of ectopic silver scale ultrastructure and pigmentation in *apA* and *Ubx B. anynana* crispants

(A–E) Optical microscopy images of the abwing (A–E) and adwing (A′–E′) surfaces, SEM images of the abwing surface (A″–E″), reflectance (A‴–E‴), and absorbance spectra (A⁗–E⁗) of the *apA* forewing control brown scales, ectopic silver and gland scales and the *Ubx* hindwing control brown scales and ectopic silver scales, respectively. The control scales for these crispants are from the same wings as the ectopic scales, close to the mosaic crispant patches.

(F) Violin plots of the upper and lower lamina thickness of the control brown scales and the ectopic silver and gland scales of *apA* and *Ubx* crispants.

(G) Area of open upper lamina of the different control and ectopic scales. Boxplots show the median, inner, and outer quartiles and whiskers up to 1.5 times the inter-quartile range. Means sharing a letter are not significantly different (Tukey-adjusted comparisons). Scale bars: (A), (A′–E), and (E′) are 20 μm and (A″–E″) are 2 μm.

opposite to those seen when silver scales became brown. Ectopic silver scales gained a closed upper lamina and an enclosed air layer, reduced their lower lamina thickness, and lost pigmentation compared with control brown scales (Figures 4A″–4E″, 4F, and 4G). The upper lamina transformation was complete for the *apA* and *Ubx* silver scale types, whereas many of the *apA* ectopic gland scales exhibited a partial transformation, having a significantly greater percentage of upper lamina open (post hoc tests from LME, adjusted p values <0.01; Tables S1 and S2 and Figure 4G). The greater variability in the ultrastructural transformations and pigmentation of the *apA* ectopic silver scale types explains the greater variability in the abwing reflectance spectra measured from these crispant scales (Figures 4B‴ and 4C″). All ectopic silver scale types exhibited a significant decrease in lower lamina thickness compared with the control brown scales (Figure 4F; post hoc tests from LME: adjusted p values <0.0001; Tables S3 and S4).

DISCUSSION AND CONCLUSION

Metallic scales in *Bicyclus anynana* are undulatory broadband reflectors

We characterized five different metallic reflectors in *B. anynana* butterflies. All five metallic scale types produced broadband silver reflectance from an undulatory bilaminate structure achieved by the closure of the "open" windows present in typical wing scales. The air gap layer of varying thickness sandwiched between two thin chitinous laminas is spatially tuned to reflect different wavelengths of light, resulting in a specular broadband metallic color in the far-field due to additive color mixing. Such an ultrastructural modification involving the gain of a contiguous upper lamina leading to metallic coloration has been well documented in multiple butterfly species across different families (Ren et al., 2020; Vukusic et al., 2009), suggesting that the convergent evolution of metallic reflectors in butterflies can occur repeatedly with a few simple modifications to the basic scale architecture. Our modeling demonstrated that although butterflies can achieve broadband metallic colors by tuning just the lower lamina, the bilaminate three-layer system comprising a sandwiched air layer between chitinous laminas is substantially brighter, perhaps explaining its repeated evolutionary origin (Ren et al., 2020). Moreover, the varying thickness of the air layer was the most important structural parameter to produce a nearly flat (smoothed out) broadband reflectance, while the upper and lower lamina thicknesses were more optimized for enhancing the broadband reflectivity. Pigmentation levels were low overall but varied among the different silver scales along with slight variations in the total open area of the upper lamina. This intriguingly suggests that the amount of pigmentation may be directly impacting the formation of the upper lamina, as previously demonstrated in other scale types of *B. anynana* (Matsuoka and Monteiro, 2018). We were unable to characterize the exact pigment composition in these scales, but the absorbance spectra of the gray-silver scales suggests that the pigments are not purely melanins but could instead be a combination of melanins and additional pigments such as ommochromes (Wasik et al., 2014).

Each of the five genes that led to gains and losses of metallic reflectance also changed pigmentation levels and scale ultrastructure dimensions

We discovered that disruptions to the five genes investigated (*Antp*, *dsx*, *apA*, *Ubx*, *and optix*) lead to a simultaneous change in scale features including pigmentation and ultrastructure dimensions. Transformation of metallic silver scales into brown scales in *Antp*, *dsxM*, *apA*, and *optix* crispants involved the loss of an upper lamina, a gain in pigmentation levels, and an increase in lower lamina thickness. This was generally true except in the case of the gray-silver scales of the hindwing, where transformation to brown scales led to a decrease in pigmentation. Conversely, gain of silver reflectance in scales of *apA* and *Ubx* crispants was accompanied by the appearance of a continuous upper lamina, a decrease in pigmentation levels, and a decrease in the thickness of the lower lamina. The breadth of variation seen in individual crispant brown scales and ectopic silver scales was potentially due to incomplete knockouts and variation in the protein function of each mutant allele. This was especially the case with *apA* crispants, possibly due to the incomplete knockout of these genes in individual scales cells.

The gain and loss of an upper lamina with concurrent changes in the thickness of the lower lamina suggests a possible conservation of total chitin production within a cell but variable deposition between the two laminas. There is some evidence for this in the forewing silver and gland scales but not in the hindwing silver scale types. The summed thicknesses of the two laminas in the WT forewing silver scales and ectopic silver scales was similar to the lower lamina thickness of the forewing control brown scales and crispant brown scales. Although there is some indication of conservation of chitin production within a single cell, testing this proposition in the future will require finer measurements of chitin production within different scale color types. Furthermore, Matsuoka and Monteiro (Matsuoka and Monteiro, 2018) speculated that downstream effector genes such as *yellow* could affect cuticle polymerization around crossribs to create windows, because *yellow B. anynana* crispant black and brown scales exhibited an upper lamina covering the windows. Given the low amounts of pigmentation seen in the different silver scale types, it is possible that the gene *yellow* is not highly expressed in silver scales, mirroring *yellow* crispant scales; *yellow* would then be a potential downstream target that would be repressed by the silver scale differentiation program. This hypothesis could be tested by measuring levels of *yellow* expression in the different colored versus silver scales of *B. anynana* as well as in crispant individuals during development.

Antp and *optix* are high-level regulators in the differentiation of silver scales, affecting both scale color and shape

Investigation of the mutant brown scales in *Antp* crispants uncovered an important role for this gene in determining a rounded scale morphology. Scales on the posterior ventral forewing and anterior dorsal hindwing of both sexes of *B. anynana*, a region where Antp is strongly expressed (Figure S7), normally have rounded distal ends, appearing silver in males and shades of brown in females. In *Antp* crispants, the rounded scales developed serrated distal tips in both sexes, concurrent with the

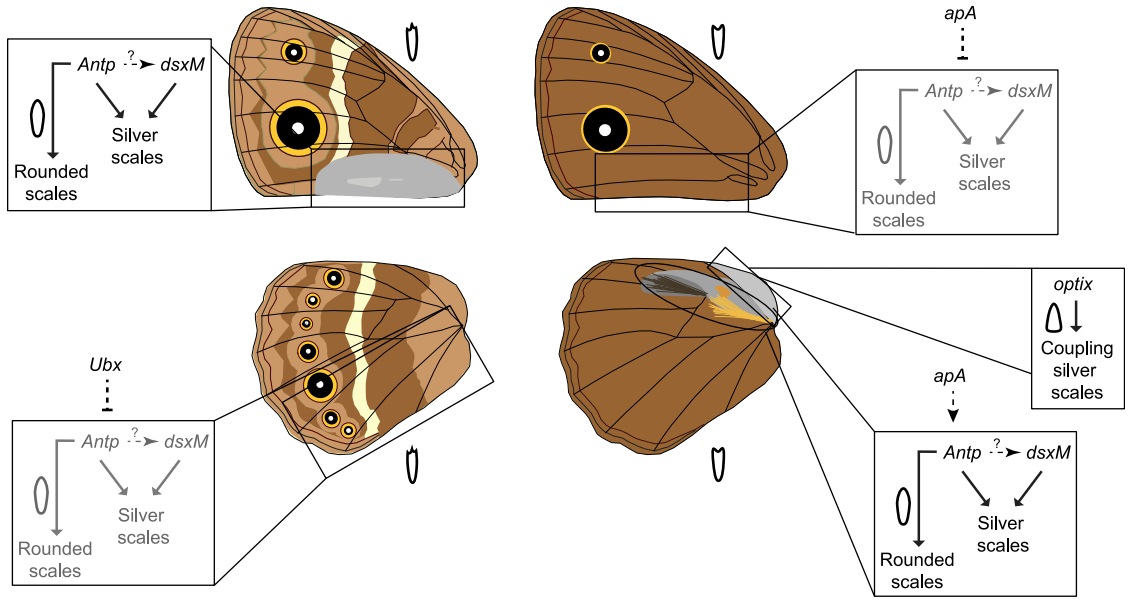

Figure 5. Functions and interactions of genes involved in the differentiation of different silver scale types across wing regions of a male *B. anynana*

For each wing region, the genes involved in differentiating silver scales and their interactions and functions are indicated within boxes. The homeotic selector genes *apA* and *Ubx* are outside the boxes. Their relation to the differentiation of silver scales is indicated by dotted lines because a direct or indirect interaction between *apA*/*Ubx* and the genes within the boxes remains unknown. The scale schematics inside the boxes represent the scale shape when the "rounded scales" part of the network is active (dark lines). Repressed parts of the network are in gray. The scale schematics outside the boxes, next to each wing surface, reflect the scale shape generally found on that surface otherwise.

transformation of silver to brown color in males only. These crispant brown scales with serrated edges resembled scales usually found on the rest of the ventral forewing (Figures S6A and S6B) or dorsal hindwing (Figures S6C and S6D), indicating that *Antp* is necessary for converting a serrated distal scale edge into a rounded scale. In contrast, whereas both *Antp* and *dsxM* affected scale color, knockout of *dsxM* did not affect scale shape. Thus, although both genes are expressed in a trait-specific manner, *Antp* affects aspects of scale color and shape, whereas *dsxM* has more restrictive transformations of color only. The exact hierarchy of interaction between *Antp* and *dsxM* in silver scale differentiation remains to be tested. Both genes could be acting in parallel or *Antp* could be upstream of *dsxM* (Figure 5). Similarly to *Antp*, *optix* also exhibits high levels of expression in a trait-specific manner, i.e., in the coupling scales, and is necessary in determining both color and shape of the coupling scales. These data suggest that *Antp* and *optix* are important regulators in the differentiation of various silver scale types. Both genes are highly expressed in the silver scale cells and affect multiple aspects of their development including the color and the morphology. Both genes are necessary for silver scale development but are not sufficient given that both *Antp* and *optix* have other expression domains on the wing like the eyespot centers (*Antp*) or the gold ring (*optix*), which are not silver. Furthermore, the conserved expression and function of *optix* in coupling scales in several other butterfly species implicates a conserved role for this gene in the development of trowel-shaped coupling scales (Martin et al., 2014; Zhang et al., 2017).

Interestingly, the metallic silver scales on male forewings and hindwings fall into two populations with different aspect ratios: the shorter silver scales covering most of the region and the longer, thin gland scales that cover only the underlying pheromone glands (Dion et al., 2016). The spatially defined occurrence of the long, thin gland scales is likely specified by the spatially restricted expression of some unknown gland-specific gene, downstream of DsxM in the silver scale differentiation program. In addition, the difference in levels of Antp protein expression between the silver and gray-silver scale regions suggests that varying thresholds of this protein are functionally relevant in the two scale types.

The unusual ridge and crossrib orientation, almost orthogonal to the normal orientation, seen in a few *Antp* crispant brown scales, hinted at a role for this gene in ridge patterning during the early stages of scale development. In developing scales, the positioning and orientation of ridges are determined by the spacing of F-actin filaments that emanate from the base of the scale, parallel to the scale's long axis (Day et al., 2019; Dinwiddie et al., 2014). The disrupted and abrupt change in orientation of the ridges and their corresponding crossribs in the *Antp* crispant scales suggests a potential disruption of the orientation of F-actin filaments. On the basis of the distal domain of occurrence of the unusual ridge patterns, along with the rounded to serrated distal edge change seen in *Antp* crispants, we speculate that *Antp* regulates the distal expression of an unknown factor, possibly a cytoskeletal component, that determines scale morphology and ridge/crossrib orientation. Hox genes such as *Abd-B* have been identified to activate cytoskeletal components

like cadherins in the development of posterior spiracles of *Drosophila* (Lovegrove et al., 2006). Furthermore, *Ubx* directly regulates cytoskeletal components such as actin and contributes to cytoskeletal reorganization in haltere cells (Pavlopoulos and Akam, 2011). In that context, our results identify a post-embryonic role of a Hox gene in the determination of the shape of a single cell. How *Antp* directs scale shape and ridge orientation, and which genes are its downstream targets, remain exciting avenues for future work.

Homeotic genes and the differentiation of silver scales

As predicted in our hypothesis, transformed scales investigated in the *apA* and *Ubx* crispants exhibited changes in both color and shape that resembled the WT silver or brown scales in that region. However, this level of transformation was similar to those observed in *Antp* and *optix* crispant scales, which are genes expressed specifically in silver scales. Given that both *apA* and *Ubx* have broad expression domains in the dorsal wing compartment (*apA*) (Prakash and Monteiro, 2018) or hindwings (*Ubx*) (Matsuoka and Monteiro, 2021) of *B. anynana*, these genes may not constitute part of the silver scale differentiation program. Nevertheless, these selector genes are likely regulating the wing and surface-specific expression of genes like *Antp*, *dsx*, and *optix* by binding to trait-specific enhancers of these genes in a combinatorial manner with other transcription factors. Searching for *apA* or *Ubx* binding sites in regulatory regions around *Antp* or *optix* and functionally testing them via targeted deletions of these regions is one way of answering this question in the future. In any case, *Ubx*, in particular, appears to repress the differentiation of silver scales on the hindwings of *B. anynana*, whereas *apA* has either a repressive or an activating function for silver scale differentiation on the forewings and hindwings, respectively (Figure 5). The direct or indirect nature of these interactions remains unknown.

Limitations of the study

This study characterized WT silver scales in the butterfly *B. anynana* and crispants of five genes to investigate their roles in the differentiation of silver scales. On the basis of this approach, we proposed potential interactions between the different genes involved in silver scale differentiation. However, one limitation of this study is that the interactions remain untested. For example, it remains unclear whether DsxM acts in parallel with or downstream of Antp in regulating silver scale differentiation. This will require investigation of how disruptions to one gene affects the expression of the other gene. A second limitation is the unclear mechanism whereby Antp regulates cell shape. This will require identification of the downstream targets of Antp and cell biological studies to determine how cell shape is regulated.

STAR★METHODS

Detailed methods are provided in the online version of this paper and include the following:

SUPPLEMENTAL INFORMATION

Supplemental information can be found online at https://doi.org/10.1016/j.celrep.2022.111052.

ACKNOWLEDGMENTS

We thank Yuji Matsuoka for providing us the *Antp* and *Ubx* crispants and Emilie Dion for helpful discussions on the statistics. We are grateful to Dr. Robert Reed for providing us the Optix antibody. We thank Sree Vaishnavi Sundararajan and Gianluca Grenci (MBI) for access and help with SEM, and the Pennycook group (MSE) for use of FIB-SEM. This research was supported by the National Research Foundation (NRF) Singapore under the Competitive Research Program (NRF-CRP20-2017-0001 Award) and the National University of Singapore.

AUTHOR CONTRIBUTIONS

A.P. and A.M. conceived and designed the study. A.P., C.F., and V.S. collected the spectral measurements. A.P. and C.F. collected the SEM data, and C.F. collected the FIB-SEM data. V.S. performed the theoretical modeling. A.P. analyzed all the data and did the Antp immunostainings. T.D.B. performed the Optix immunostainings and the *optix* knockout experiments. A.P. wrote the manuscript with inputs from all the authors.

DECLARATION OF INTERESTS

The authors declare no competing interests.

Received: February 11, 2022
Revised: May 6, 2022
Accepted: June 14, 2022
Published: July 5, 2022

REFERENCES

Banerjee, T.D., Shan, S.K., and Monteiro, A. (2021). *Optix* is involved in eyespot development via a possible positional information mechanism. Preprint at bioRxiv. https://doi.org/10.1101/2021.05.22.445259.

D'Alba, L., Wang, B., Vanthournout, B., and Shawkey, M.D. (2019). The golden age of arthropods: ancient mechanisms of colour production in body scales. J. R. Soc. Interface *16*. https://doi.org/10.1098/rsif.2019.0366.

Day, C.R., Hanly, J.J., Ren, A., and Martin, A. (2019). Sub-micrometer insights into the cytoskeletal dynamics and ultrastructural diversity of butterfly wing scales. Dev. Dyn. *248*, 657–670. https://doi.org/10.1002/dvdy.63.

Denton, E.J. (1970). Review lecture: on the organization of reflecting surfaces in some marine animals. Philos. Trans. R. Soc. Lond. Ser. B Biol. Sci. *258*, 285–313. https://doi.org/10.1098/rstb.1970.0037.

Denton, E.J., and Land, M.F. (1971). Mechanism of reflexion in silvery layers of fish and cephalopods. Proc. R. Soc. Lond. Ser. B Biol. Sci. *178*, 43–61. https://doi.org/10.1098/rspb.1971.0051.

Dinwiddie, A., Null, R., Pizzano, M., Chuong, L., Leigh Krup, A., Ee Tan, H., and Patel, N.H. (2014). Dynamics of F-actin prefigure the structure of butterfly wing scales. Dev. Biol. *392*, 404–418. https://doi.org/10.1016/j.ydbio.2014.06.005.

Dion, E., Monteiro, A., and Yew, J.Y. (2016). Phenotypic plasticity in sex pheromone production in Bicyclus anynana butterflies. Sci. Rep. *6*, 1–13. https://doi.org/10.1038/srep39002.

Dolinko, A., Borgmann, L., Lutz, C., Curticean, E.R., Wacker, I., Vidal, M.S., Szischik, C., Donie, Y., Inchaussandague, M., Skigin, D., et al. (2021). Analysis of the optical properties of the silvery spots on the wings of the Gulf Fritillary, Dione vanillae. Sci. Rep. *11*, 19341. https://doi.org/10.1038/s41598-021-98237-9.

Finlayson, E.D., McDonald, L.T., and Vukusic, P. (2017). Optically ambidextrous circularly polarized reflection from the chiral cuticle of the scarab beetle Chrysina resplendens. J. R. Soc. Interface *14*. https://doi.org/10.1098/rsif.2017.0129.

Gur, D., Nicolas, J.-D., Brumfeld, V., Bar-Elli, O., Oron, D., and Levkowitz, G. (2018). The dual functional reflecting Iris of the zebrafish. Adv. Sci. *5*, 1800338. https://doi.org/10.1002/advs.201800338.

Holt, A.L., Sweeney, A.M., Johnsen, S., and Morse, D.E. (2011). A highly distributed Bragg stack with unique geometry provides effective camouflage for Loliginid squid eyes. J. R. Soc. Interface *8*, 1386–1399. https://doi.org/10.1098/rsif.2010.0702.

Hothorn, T., Bretz, F., and Westfall, P. (2008). Simultaneous inference in general parametric models. Biom. J. *50*, 346–363.

Johnsen, S. (2014). Hide and seek in the open sea: pelagic camouflage and visual countermeasures. Ann. Rev. Mar. Sci *6*, 369–392. https://doi.org/10.1146/annurev-marine-010213-135018.

Kilchoer, C., Steiner, U., and Wilts, B.D. (2019). Thin-film structural coloration from simple fused scales in moths. Interface Focus *9*. https://doi.org/10.1098/rsfs.2018.0044.

Kinoshita, M., Sato, M., and Arikawa, K. (1997). Spectral receptors of nymphalid butterflies. Naturwissenschaften *84*, 199–201. https://doi.org/10.1007/s001140050377.

Kinoshita, S., Yoshioka, S., and Miyazaki, J. (2008). Physics of structural colors. Reports Prog. Phys. *71*. https://doi.org/10.1088/0034-4885/71/7/076401.

Land, M.F. (1972). The physics and biology of animal reflectors. Prog. Biophys. Mol. Biol. *24*, 75–106. https://doi.org/10.1016/0079-6107(72)90004-1.

Livraghi, L., Hanly, J.J., Van Bellghem, S.M., Montejo-Kovacevich, G., van der Heijden, E.S.M., Loh, L.S., Ren, A., Warren, I.A., Lewis, J.J., Concha, C., et al. (2021). Cortex cis-regulatory switches establish scale colour identity and pattern diversity in heliconius. Elife *10*, 1–31. https://doi.org/10.7554/eLife.68549.

Lovegrove, B., Simões, S., Rivas, M.L., Sotillos, S., Johnson, K., Knust, E., Jacinto, A., and Hombría, J.C.G. (2006). Coordinated control of cell adhesion, polarity, and cytoskeleton underlies hox-induced organogenesis in Drosophila. Curr. Biol. *16*, 2206–2216. https://doi.org/10.1016/j.cub.2006.09.029.

Maia, R., Gruson, H., Endler, J.A., and White, T.E. (2019). pavo 2: New tools for the spectral and spatial analysis of colour in r. Methods Ecol. Evol. *10*, 1097–1107. https://doi.org/10.1111/2041-210X.13174.

Martin, A., McCulloch, K.J., Patel, N.H., Briscoe, A.D., Gilbert, L.E., and Reed, R.D. (2014). Multiple recent co-options of Optix associated with novel traits in adaptive butterfly wing radiations. EvoDevo *5*, 1–13. https://doi.org/10.1186/2041-9139-5-7.

Matsuoka, Y., and Monteiro, A. (2018). Melanin pathway genes regulate color and morphology of butterfly wing scales. Cell Rep. *24*, 56–65. https://doi.org/10.1016/j.celrep.2018.05.092.

Matsuoka, Y., and Monteiro, A. (2021). Hox genes are essential for the development of eyespots in Bicyclus anynana butterflies. Genetics *217*. https://doi.org/10.1093/genetics/iyaa005.

McKenzie, D.R., Yin, Y., and McFall, W.D. (1995). Silvery fish skin as an example of a chaotic reflector. Proc. R. Soc. Lond. Ser. A Math. Phys. Sci. *451*, 579–584. https://doi.org/10.1098/rspa.1995.0144.

Nan, S.N., Cheng-Chia, T., Fernando, C., Bernard, G.D., Nanfang, Y., and Rüdiger, W. (2015). Keeping cool: enhanced optical reflection and radiative heat dissipation in Saharan silver ants. Science *349*, 298–301. https://doi.org/10.1126/science.aab3564.

Neville, A.C. (1977). Metallic gold and silver colours in some insect cuticles. J. Insect Physiol. *23*, 1267–1274. https://doi.org/10.1016/0022-1910(77)90069-5.

Parker, a. R., McKenzie, D.R., and Large, M.C.J. (1998). Multilayer reflectors in animals using green and gold beetles as contrasting examples. J. Exp. Biol. *201*, 1307–1313.

Pavlopoulos, A., and Akam, M. (2011). Hox gene Ultrabithorax regulates distinct sets of target genes at successive stages of Drosophila haltere morphogenesis. Proc. Natl. Acad. Sci. USA *108*, 2855–2860. https://doi.org/10.1073/pnas.1015077108.

Pinheiro, J., Bates, D., DebRoy, S., and Sarkar, D.; R Core Team (2021). nlme: Linear and nonlinear mixed effects models (R package version 3.1-152). https://CRAN.R-project.org/package=nlme.

Prakash, A., and Monteiro, A. (2018). *Apterous A* specifies dorsal wing patterns and sexual traits in butterflies. Proc. R. Soc. B Biol. Sci. *285*, 20172685. https://doi.org/10.1098/rspb.2017.2685.

Prakash, A., and Monteiro, A. (2020). Doublesex mediates the development of sex-specific pheromone organs in Bicyclus butterflies via multiple mechanisms. Mol. Biol. Evol. *37*, 1694–1707. https://doi.org/10.1093/molbev/msaa039.

Qingqing, Z., Wolfram, M., Jörg, A., Ansorge, T.A., Timothy, M.L., Mcnamara, M.E., Jarzembowski, E.A., Wilfried, W., Richard, K., Xiaoyin, R., et al. (2021). Fossil scales illuminate the early evolution of lepidopterans and structural colors. Sci. Adv. *4*, e1700988. https://doi.org/10.1126/sciadv.1700988.

R Core Team. (2021). R: A Language and Environment for Statistical Computing.

Ren, A., Day, C.R., Hanly, J.J., Counterman, B.A., Morehouse, N.I., and Martin, A. (2020). Convergent evolution of broadband reflectors underlies metallic coloration in butterflies. Front. Ecol. Evol. *8*, 206.

Schneider, C.A., Rasband, W.S., and Eliceiri, K.W. (2012). NIH Image to ImageJ: 25 years of image analysis. Nat. Methods *9*, 671–675. https://doi.org/10.1038/nmeth.2089.

Seago, A.E., Brady, P., Vigneron, J.-P., and Schultz, T.D. (2009). Gold bugs and beyond: a review of iridescence and structural colour mechanisms in beetles (Coleoptera). J. R. Soc. Interface *6*, S165–S184. https://doi.org/10.1098/rsif.2008.0354.focus.

Siddique, R.H., Vignolini, S., Bartels, C., Wacker, I., and Hölscher, H. (2016). Colour formation on the wings of the butterfly Hypolimnas salmacis by scale stacking. Sci. Rep. *6*, 36204. https://doi.org/10.1038/srep36204.

Simonsen, T.J. (2007). Comparative morphology and evolutionary aspects of the reflective under wing scale-pattern in Fritillary butterflies (Nymphalidae: Argynnini). Zool. Anz. *246*, 1–10. https://doi.org/10.1016/j.jcz.2005.04.005.

Srinivasarao, M. (1999). Nano-optics in the biological world: beetles, butterflies, birds, and moths. Chem. Rev. *99*, 1935–1962. https://doi.org/10.1021/cr970080y.

Stavenga, D.G., Leertouwer, H.L., Osorio, D.C., and Wilts, B.D. (2015). High refractive index of melanin in shiny occipital feathers of a bird of paradise. Light Sci. Appl. *4*, e243. https://doi.org/10.1038/lsa.2015.16.

Steinbrecht, R.a., Mohren, W., Pulker, H.K., and Schneider, D. (1985). Cuticular interference reflectors in the golden pupae of danaine butterflies. Proc. R. Soc. B Biol. Sci. *226*, 367–390. https://doi.org/10.1098/rspb.1985.0100.

Steinbrecht, R.A. (1985). Fine structure and development of the silver and golden cuticle in butterfly pupae. Tissue Cell *17*, 745–762. https://doi.org/10.1016/0040-8166(85)90008-4.

Tendolkar, A., Pomerantz, A.F., Heryanto, C., Shirk, P.D., Patel, N.H., and Martin, A. (2021). Ultrabithorax is a micromanager of hindwing identity in butterflies and moths. Front. Ecol. Evol. *9*. https://doi.org/10.3389/fevo.2021.643661.

Thayer, R.C., Allen, F.I., and Patel, N.H. (2020). Structural color in Junonia butterflies evolves by tuning scale lamina thickness. Elife *9*, e52187. https://doi.org/10.7554/eLife.52187.

Vanthournout, B., Rousaki, A., Parmentier, T., Janssens, F., Mertens, J., Vandenabeele, P., D'Alba, L., and Shawkey, M. (2021). Springtail coloration at a finer scale: mechanisms behind vibrant collembolan metallic colours. J. R. Soc. Interface *18*, 20210188. https://doi.org/10.1098/rsif.2021.0188.

Vukusic, P., and Sambles, J.R. (2003). Photonic structures in biology. Nature *424*, 852–855. https://doi.org/10.1038/nature01941.

Vukusic, P., Kelly, R., and Hooper, I. (2009). A biological sub-micron thickness optical broadband reflector characterized using both light and microwaves. J. R. Soc. Interface *6*, S193–S201. https://doi.org/10.1098/rsif.2008.0345.focus.

Wagner, H.-J., Douglas, R.H., Frank, T.M., Roberts, N.W., and Partridge, J.C. (2009). A novel vertebrate eye using both refractive and reflective optics. Curr. Biol. *19*, 108–114. https://doi.org/10.1016/j.cub.2008.11.061.

Wasik, B.R., Liew, S.F., Lilien, D.A., Dinwiddie, A.J., Noh, H., Cao, H., and Monteiro, A. (2014). Artificial selection for structural color on butterfly wings and comparison with natural evolution. Proc. Natl. Acad. Sci. USA *111*, 12109–12114. https://doi.org/10.1073/pnas.1402770111.

Weatherbee, S.D., Frederik Nijhout, H., Grunert, L.W., Halder, G., Galant, R., Selegue, J., and Carroll, S. (1999). Ultrabithorax function in butterfly wings and the evolution of insect wing patterns. Curr. Biol. *9*, 109–115. https://doi.org/10.1016/S0960-9822(99)80064-5.

Wilts, B.D., Pirih, P., Arikawa, K., and Stavenga, D.G. (2013). Shiny wing scales cause spec(tac)ular camouflage of the angled sunbeam butterfly, Curetis acuta. Biol. J. Linn. Soc. *109*, 279–289. https://doi.org/10.1111/bij.12070.

Zhang, L., Mazo-Vargas, A., and Reed, R.D. (2017). Single master regulatory gene coordinates the evolution and development of butterfly color and iridescence. Proc. Natl. Acad. Sci. USA *114*, 10707–10712. https://doi.org/10.1073/pnas.1709058114.

STAR★METHODS

KEY RESOURCES TABLE

REAGENT or RESOURCE	SOURCE	IDENTIFIER
Antibodies		
Mouse anti-Antp 4C3	DSHB	Cat# anti-Antp 4C3; RRID:AB_528082
Rat anti-optix	A gift from Dr. Robert Reed	N/A
Alexa Fluor 488 AffiniPure Goat anti-mouse IgG	Jackson ImmunoResearch Labs	Cat# 115-545-003; RRID:AB_2338840
Alexa Fluor 488 Goat anti-rat IgG secondary antibody	Thermo Fisher Scientific	Cat# A-11006; RRID:AB_2534074
Deposited data		
Code for performing the broadband reflectance simulations	This paper	https://github.com/evolphotonics/bbandAgmodel https://doi.org/10.5281/zenodo.5602246
Scale ultrastructure measurements	This paper	Table S5 - source data
Experimental models: organisms/strains		
Bicyclus anynana wildtype butterflies	Antonia Monteiro lab	N/A
Bicyclus anynana apA crispants	Prakash and Monteiro (2018)	https://doi.org/10.1098/rspb.2017.2685
Bicyclus anynana dsx crispants	Prakash and Monteiro (2020)	https://doi.org/10.1093/molbev/msaa039
Bicyclus anynana Ubx crispants	Matsuoka and Monteiro (2021)	https://doi.org/10.1093/genetics/iyaa005
Bicyclus anynana Antp crispants	Matsuoka and Monteiro (2021)	https://doi.org/10.1093/genetics/iyaa005
Bicyclus anynana optix crispants	Das Banerjee et al., Biorxiv	https://doi.org/10.1101/2021.05.22.445259
Oligonucleotides		
Guide RNA sequences to generate the different *Bicyclus anynana* crispants	Compiled in this paper	Table S6
Software and algorithms		
R Studio 1.4.1106 with R 4.0.4	R core team	https://www.rstudio.com/; https://www.r-project.org/
FreeSnell	A. Jaffer	http://people.csail.mit.edu/jaffer/FreeSnell
ImageJ 1.52a (Java 1.8.0_112)	Schneider et al. (2012)	https://imagej.nih.gov/ij/

RESOURCE AVAILABILITY

Lead contact

Further information and requests for resources and reagents should be directed to and will be fulfilled by the lead contact, Antonia Mónteiro (antonia.monteiro@nus.edu.sg).

Materials availability

All resources and reagents generated in this study are listed in this paper or are available upon request to the lead contact.

Data and code availability

- All data generated in this paper are available in the Supplementary excel file and, analyses are reported in the methods. They are publicly available as of the date of publication.
- All original code has been deposited at GitHub with a Zenodo DOI and is publicly available as of the date of publication. Links are provided in the key resources table.
- Any additional information required to reanalyze the data reported in this paper is available from the lead contact upon request.

EXPERIMENTAL MODEL AND SUBJECT DETAILS

Crispant individuals and sampled scale types

B. anynana crispants for *apterous A* (*apA*) (Prakash and Monteiro, 2018), *Ultrabithorax* (*Ubx*) (Matsuoka and Monteiro, 2021), *doublesex* (*dsx*) (Prakash and Monteiro, 2020) and *Antennapedia* (*Antp*) (Matsuoka and Monteiro, 2021) were previously generated in our lab

by CRISPR-Cas9 mediated gene editing. Crispants for *optix* were generated by injections of two guide RNAs targeting the *optix* coding sequence (Banerjee et al., 2021). guide RNA sequences and regions targeted are compiled in Table S6. Five different silver scale types were sampled, namely, the silver and the gland scales on the androconial patch of male ventral forewings, the silver and grey-silver scales near the androconial patches of male dorsal hindwings and the coupling scales near the base of the dorsal hindwing in females (Figure 1A).

METHOD DETAILS

Scanning electron microscopy

Five to six scales from different regions of the crispant individuals (Figure 1A) were individually mounted onto carbon tape and sputter coated with gold using a JFC-1100 Fine Coat Ion Sputter (JEOL Ltd. Japan). Images were obtained using a JEOL JSM-6510LV scanning electron microscope (JEOL Ltd. Japan). For the wildtype, *apA* and *dsx* crispants, three different individuals were sampled for each case. Two individuals were sampled for *Antp* and *optix* crispants while only one crispant was obtained for *Ubx*.

Percentage area of open upper lamina measurements

From the SEM images, the percentage of area of open upper lamina was calculated using ImageJ 1.52a (Java 1.8.0_112) (Schneider et al., 2012). A 20 μm^2 (10 μm^2 for gland scales) region of interest was defined approximately at the center of the scale and the region outside cleared. A thresholding was applied based on the values of the bright (ridge and crossribs) and dark (windows) regions of the SEM. The dark areas were selected and added to the ROI Manager in ImageJ using the Analyze Particles function. The selected regions were combined using the OR function in the ROI Manager. The combined area of the open upper lamina within the defined regions was measured and converted into a percentage.

Focused ion beam scanning electron microscopy (FIB-SEM)

FIB-SEM was used to measure the lower lamina, upper lamina, and air gap thicknesses for all scale types in our analysis and corrected for tilted perspective (measured thickness/sin 52°). Briefly, samples were prepared by sputter-coating with platinum to increase conductivity. The scales were milled using a gallium ion beam on a FEI Versa 3D with the following settings: beam voltage −8kV, beam current −12pA at a 52° tilt. Image acquisition was performed in the same equipment with the following settings: beam voltage −5kV, beam current −13pA. Milling was done at the center of each scale. Thickness measurements were done in ImageJ. For each scale type, ten measurements were taken per scale with 3–16 scales sampled from 1 to 2 individuals. Measurements were made along most of the lower lamina which is uniform, excluding the region around the ridge base, where the thickness is highly variable.

Optical imaging and UV-VIS-NIR microspectrophotometry

Light microscope images of individual scales were recorded using the 20X lens of a uSight-2000-Ni microspectrophotometer (Technospex Pte. Ltd., Singapore) and a Touptek U3CMOS-05 camera. Scales were individually mounted on a glass slide or in a refractive index matching medium (clove oil) and multiple images at different focal planes (z stack) were obtained. Stacking was done in Adobe Photoshop v 22.5.1 (Adobe, California, USA).

Normal-incidence UV-VIS-NIR reflectance spectra of scales were acquired using the same microspectrophotometer setup but with a 100x objective. Spectra with usable range between 335 and 950 nm were collected using a high NA 100x objective from a ~2 μm sized spot (100 ms integration time, 10x averaging) and calibrated using an Avantes WS-2 reference tile made of white diffuse polytetrafluoroethylene. Individual scales were mounted on a black carbon tape and illuminated with a Mercury-Xenon lamp (ThorLabs Inc., New Jersey, USA). Measurements were taken from both abwing and adwing surfaces. For each scale type, measurements from five to ten individual scales from one individual were averaged. Absorbance spectrum was measured for individual scales immersed in a refractive index matching liquid (clove oil) using a 20X objective. Six to eight individual measures from one individual were averaged for each crispant type and wildtype. Analysis and spectral plots were done in R Studio 1.4.1106 with R 4.0.4 (R Core Team, 2021) using the R-package *pavo* (v 2.7) (Maia et al., 2019).

Antp and optix immunostaining

The Antp primary antibody used was the same as (Matsuoka and Monteiro, 2021). anti-Antp 4C3 was deposited to the Developmental Studies Hybridoma Bank by D. Brower. The secondary antibody was an Alexa Fluor 488-conjugated goat anti-mouse antibody (Jackson ImmunoResearch Laboratories, Inc.). The Optix primary antibody (from rat) was a gift from Robert D. Reed and was the same as (Banerjee et al., 2021). The secondary antibody was an anti-rat AF 488 (Thermo Fisher, #A-11006).

Pupal wing tissues were dissected in phosphate-buffered saline (PBS) and transferred to fix buffer at room temperature (0.1M PIPES pH 6.9, 1mM EGTA pH 6.9, 1% Triton X-100, 2mM MgSO4). Wings were fixed in 4% formaldehyde (added to the wells) at room temperature for 30 min, then washed five times with PBS. Blocking was done overnight at 4°C in block buffer (50mM Tris pH 6.8, 150mM NaCl, 0.5% IGEPAL, 1mg/mL BSA). The wings were then incubated in primary antibody (1:100 of 1:1 anti-Antp:glycerol solution or 1:3000 of anti-Optix) in wash buffer (50mM Tris pH 6.8, 150mM NaCl, 0.5% IGEPAL, 1mg/mL BSA) at room temperature for 1 h, washed with wash buffer four times and then incubated with secondary antibody (1:500) for 30 min at room

temperature. Samples were washed to remove the secondary antibody and incubated with DAPI for 5–10 min, followed by further washing. Wings were imaged on an Olympus FLUOVIEW FV3000 confocal microscope.

Theoretical modeling

To model the theoretical reflectance of scale ultrastructural elements, both individually as well as in various combinations, we used the freely available FreeSnell software (A. Jaffer, http://people.csail.mit.edu/jaffer/FreeSnell), a thin-film optical simulator implemented in the SCM Scheme language. As inputs to the model, we used the upper and lower lamina and air gap thickness measurements (see Figure 1I and Table S5 – source data) from FIB-SEM cross-sectional images of the various scale types. The calculations were first performed in a hierarchical fashion – varying only upper lamina, air gap or lower lamina thickness, then both upper and lower lamina thicknesses, and lastly all three simultaneously. Our modeling suggested that only 3-layer models that include a varying air gap layer were able to explain both the broadband nature and the overall brightness of the measured scale reflectivities, as compared with 3-layer models with constant air gap thickness but varying upper and/or lower lamina thicknesses or 1-layer models with just an upper or lower lamina (see Figures S3 and S4).

We used the following variational method to generate the mean theoretical reflectance (with error bars) for the five different silver scale types reported in Figures 1B'''–1F''', and S2. For each scale type, we averaged 200 spectra generated using a 3-layer model – where only the air layer thickness parameter is varied using a set of N = 200 values specified using a normal distribution with the measured mean and standard deviation (see Figure 1I and Table S5 – source data), while the upper and lower lamina thicknesses were constant and set to their respective measured mean values. We plot the theoretical abwing spectra in Figures 1 and S2 after accounting for the short-wavelength absorption due to pigments (1B''''-F''''). Final predicted abwing reflectance were obtained by multiplying the theoretical reflectance by the corresponding percentage pigmentary transmittance (T, given by 10^{-A}, where A is the measured absorbance of the scale type).

In order to perform the systematic parametric sweeps presented as heatmaps in Figure S4, for each scale type, two of the three structural parameters were held constant and set to their measured mean values (see Figures 1I and Table S5 – source data), while the third layer thickness was allowed to vary over a range of values in small discrete steps (0–2 μm for air gap in 20 nm steps, 0 to 500 nm in 5 nm steps for both lower and upper lamina). Further at each step, we used the variational method described above to generate and average over the spectra corresponding to N = 100 values specified by a normal distribution centered on the step value (i.e. mean), and a standard deviation scaled by the coefficient of variation of the corresponding layer's measurement (step standard deviation = step mean * measured standard deviation/measured mean; for instance, the standard deviation corresponding to a mean forewing silver upper lamina thickness of 500 nm works out to be 500 nm * 8 nm/64 nm = 62.5 nm). Here, we used N = 100 in contrast to the N = 200 used earlier, in order to save computational time, and having verified that they both produced near identical mean spectra. At each step, we also averaged the mean spectra over the entire wavelength range and plotted this single value (mean broadband reflectivity, R) as a function of the varied thickness parameter as an inset (Figure S4).

Random value generation and averaging of spectra were performed using custom code written in *bash* and *awk* scripting languages. We used the stackplot functionality of *pavo* package (v 2.4) (Maia et al., 2019) in R (v 3.6.3) (R Core Team, 2021) to produce the extrapolated heatmaps in Figure S4. In order to average over any spatial differences in pigment deposition, the absorbance data were measured using a 20X objective that does not extend into the UV. The absorbance measurements were therefore extrapolated into the UV using local polynomial regression with the help of *loess* (span of 0.2) and *predict* functions in R (R Core Team, 2021). Lastly, the layer thickness measurements plotted in Figure S3C were made on a FIB-SEM cross-section image using the BAR plugin 1.5.2 (doi: 10.5281/zenodo.495245) in FIJI (v 1.5.3) running on a Linux platform. Briefly, a ~1.7 μm wide area region of interest (ROI) was selected, air region in the exposed plane masked and thresholded to convert into a binary image, and then filtered (3 × 3 median) to remove noise. A vertical line ROI was drawn at the left end of the image ROI and translated by 6 pixels (or ~20 nm) along the width of the image to the other end. At each of these 82 loci, the corresponding line profile was plotted. A horizontal line ROI was plotted at the half-height of this plot profile and subsequently its line profile plotted, in turn. The position of the air-chitin interfaces were found using the ''Find Peaks'' functionality of the BAR plugin as applied to this second-order line profile, using default parameters. These tasks were automated using a custom macro. The difference between consecutive minima gave the relevant layer thicknesses (see Table S5 - source data). The color swatch at each of the 82 line profile locations were generated by FreeSnell as 64 × 64 pixel color squares by invoking the color-swatch function that uses the CIE illuminant D65.

The entire set of code for performing the broadband reflectance simulations is publicly available in the following GitHub repository: https://github.com/evolphotonics/bbandAgmodel (https://doi.org/10.5281/zenodo.5602246).

Trichromat insect visual modeling

In order to understand how butterflies could perceive the theoretical spectra produced by the various models (Figure S3B), we performed visual modeling using *pavo* (v 2.4) (Maia et al., 2019) in R 3.6.3 (R Core Team, 2021). The relative stimulation (quantal catches) of the three photoreceptors (s, m, and l) and the corresponding colorimetric parameters in a trichromat color space (with chroma or saturation, the magnitude of the position vector given by the distance from the achromatic centroid of the color triangle) were computed and plotted with the Vinegar Fly (Diptera: *Drosophila melanogaster*) spectral sensitivities and default settings (homogeneous illuminance). This was the closest available visual model specified in *pavo* to *Bicyclus anynana* butterflies, in terms of phylogenetic relatedness (Diptera is sister to Lepidoptera) and the overall similarity of their visual sensitivities (Kinoshita et al., 1997).

QUANTIFICATION AND STATISTICAL ANALYSIS

Statistical analysis

Statistical analyses were performed in R Studio 1.4.1106 with R 4.0.4 (R Core Team, 2021). The differences in mean thickness or mean percent area of open upper lamina among the different crispant types and wildtype were analyzed using a linear mixed-effects model (LME) that allows for fixed and random effects. Due to the hierarchical nature of the datasets, where multiple measurements were taken from each scale and multiple scales were analyzed for each individual, we used an LME with the crispant type as the fixed factor, and scale nested within individual as a random factor. LME was run using the nlme package (v 3.1.152) (Pinheiro et al., 2021). In addition, due to the violation of the homogeneity of variance in the measurements among different crispant types or wildtype, we allowed for different variance structures for each type using the 'varIdent' function in the nlme package. Different models were compared using the anova function and the best model was selected using AIC as a criterion. Adjusted p-values for different pairwise comparisons were obtained by a posthoc analysis using the multcomp (v 1.4.17) package (Hothorn et al., 2008) and Tukey contrasts. Outcomes of the LME tests and the adjusted p-values for multiple comparisons for all the tests are given in Tables S1–S4.

Cell Reports, Volume *40*

Supplemental information

Antennapedia and *optix* regulate metallic silver wing scale development and cell shape in *Bicyclus anynana* butterflies

Anupama Prakash, Cédric Finet, Tirtha Das Banerjee, Vinodkumar Saranathan, and Antónia Monteiro

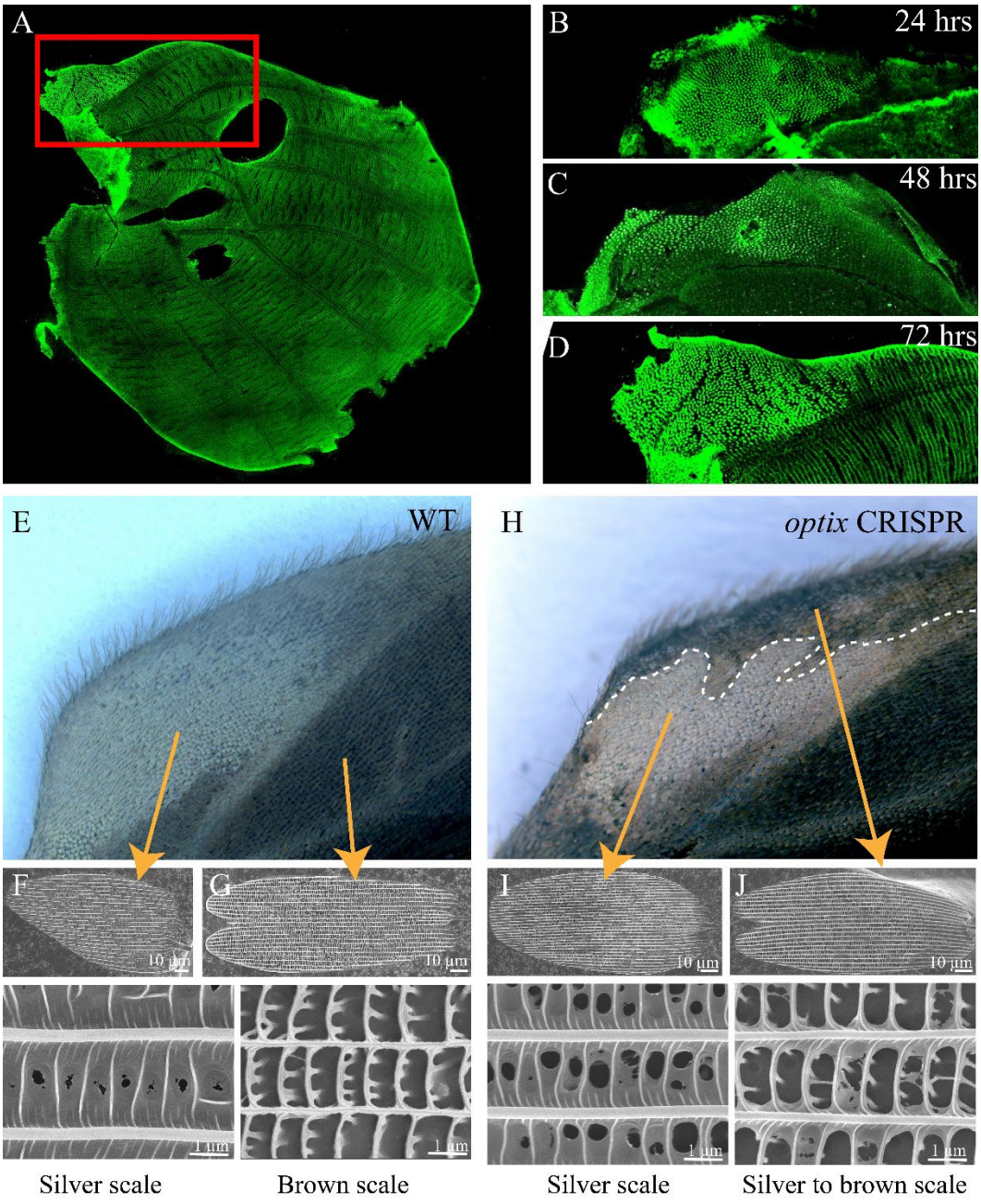

Supplementary Figure S1: Optix protein expression in the pupal hindwings of *Bicyclus anynana* and crispant phenotypes in the silver scale region. Related to section 1 of the results. (A) Hindwing showing expression of Optix proteins in the future silver scales (red box). Expression of Optix at (B) 24 hrs, (C) 48 hrs and (D) 72 hrs pupal hindwing. (E) WT hindwing (F, G) Ultrastructure of a WT silver coupling scale and a WT brown scale. (H) *optix* crispant hindwing. *optix* CRISPR results in the conversion of silver coupling scales into brown scales. (I, J) Ultrastructure of a silver coupling scale and a silver coupling scale converted into a brown scale from an *optix* crispant hindwing. The crispant brown scale structure resembles that of a WT brown scale with open windows.

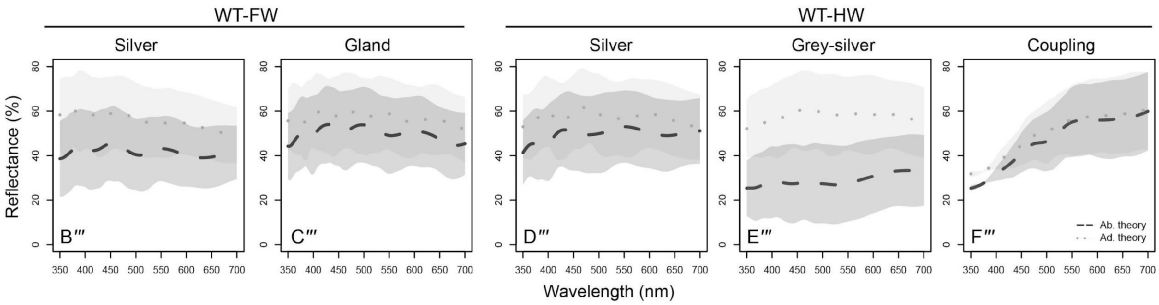

Supplementary Figure S2: Theoretically modeled reflectance spectra for the five different wildtype silver scales of *Bicyclus anynana*. Related to Figure 1. The abwing (dashed line) and adwing (dotted line) spectra are reproduced here from Fig 1B‴-F‴, along with shaded areas representing one standard deviation from the mean (dashed or dotted lines). The abwing spectra include the corresponding pigmentary absorption shown in Fig 1B⁗-F⁗. The theoretical modeled spectra which were computed with respect to a specular standard have been offset vertically (+30%) so that they are comparable to experimental reflectance measured relative to a diffuse standard (Fig 1B‴-F‴). See methods for details.

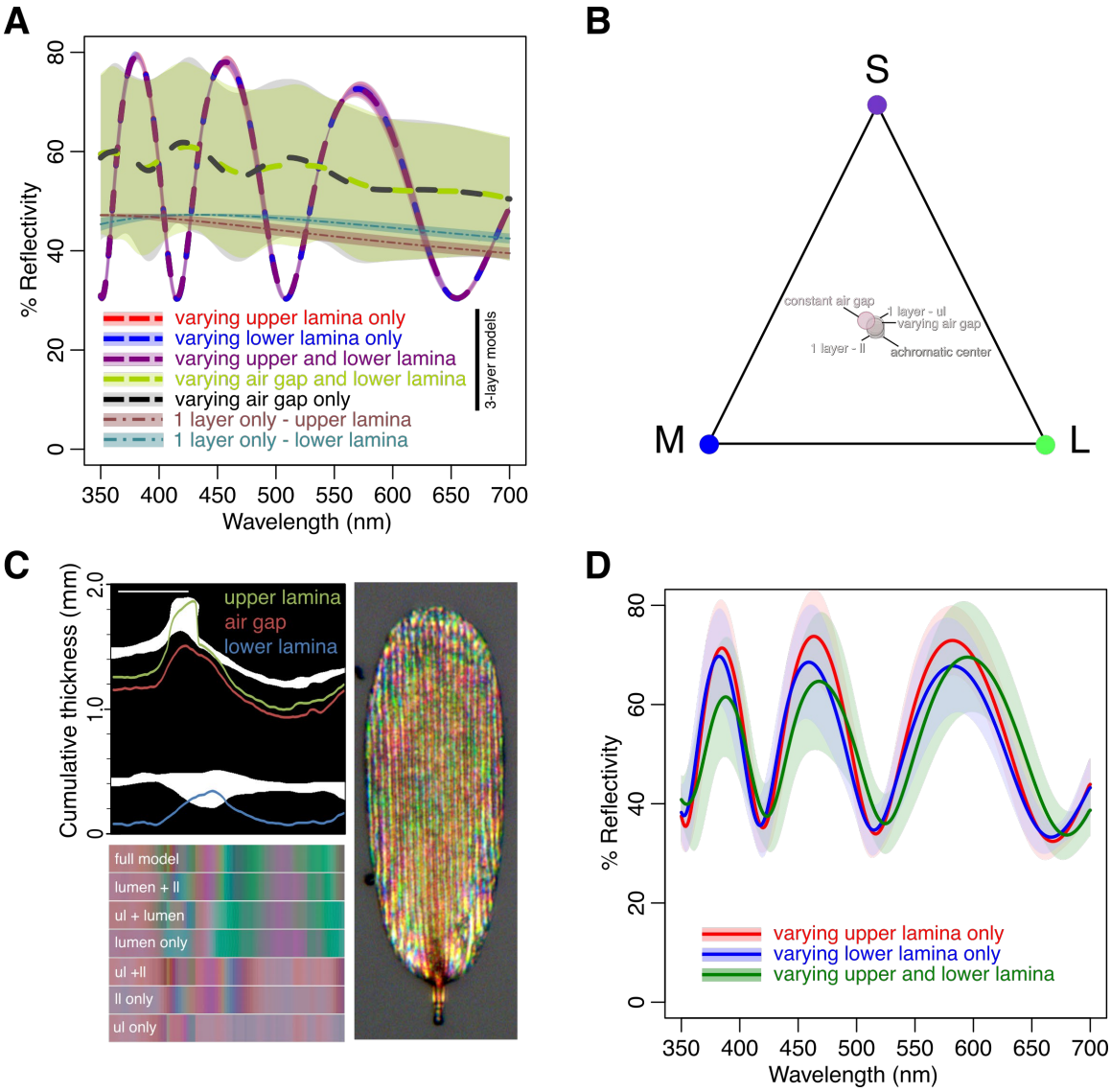

Supplementary Figure S3: Hierarchical optical modeling of the broadband metallic color production in forewing silver scales of *B. anynana*. Related to Figure 1. **A**) Mean modeled spectra are plotted for the full 3-layer models (dashed curves) and 1-layer models (dash-dot curves) using the variational method (see STAR methods for details) with shaded areas representing 1 standard deviation. For 3-layer models, either one or two specified (see legend) parameters are varied, while keeping the other parameter(s) constant. An enclosed air gap layer (lumen) of variable thickness is necessary to produce a bright, relatively flat broadband (achromatic) reflectance, compared to the rather chromatic sinusoidal spectra when air gap thickness does not change or the more broadband (flat) but much lower (duller) reflectance from a 1-layer model with only a varying upper or lower lamina. Note, the 3-layer models with a varying upper (red curve) or lower lamina (blue curve) essentially overlap, occluding the former from view. **B**) The mean modeled reflectance in **A** plotted according to a *Drosophila* trichromat visual model further affirms that only nanostructural models with varying air gap layer (grey circles) produce broadband colors that are closer to the achromatic centroid (light grey square), compared to models

where the air gap thickness is constant (pale pink circles). **C**) In contrast to the spectra in **A**, which were modelled using the mean and variance of lamina and air gap thickness measurements (Supplementary Table S5) made in the closed window areas (away from the ridges), here we model the color and spectra directly from a silver scale FIB-SEM cross-section, thereby accounting for the thickening of the laminas near the ridges. Top panel: A binarized (chitin – white, air – black) region of interest (ROI) from a scale FIB-SEM cross-section overlaid with the corresponding cumulative thickness profiles of the three layers (colored lines). Scale bar for *x*-axis (500 nm) differs from *y*-axis as the latter has been corrected for perspective foreshortening in FIB-SEM measurements. Bottom panel: 82 conjoined color swatches for each of the 7 possible hierarchical models where 1, 2 or all 3 nanostructural layers are varied are shown at ~20 nm intervals (i.e., every 6 pixels) along the width of the ROI. Right panel: An abwing light micrograph of a wild-type forewing silver scale, with the levels function enhanced in Photoshop, to illustrate the local spatial color variation. Models incorporating the varying air gap layer are closest in hue to the full 3-layer model, whereas the effects of the laminas are most pronounced at or near ridges, far from inter-ridge regions where they have nearly uniform thicknesses. The blue-green and purple-pink hues seen in the model correspond well with similar color highlights observed in the high magnification image of a silver scale shown here. **D**) Averaging the spectra corresponding to the 82 color swatches in **C** for the 1- and 2-layer lamina models understandably shows more variance as compared to **A** ($N = 200$), however, the resulting spectra here are still similarly chromatic and sinusoidal. When laminar thicknesses vary more at the ridges, interference from upper and lower lamina reduces the intensity at shorter wavelengths. This perhaps explains a similar reduction in the measured reflectivities at short wavelengths, relative to our simplified theoretical predictions that does not account for the thickening at and around ridges (Fig 1B‴-F‴, and Supp Fig S2). Abbreviations: ul – upper lamina, ll – lower lamina.

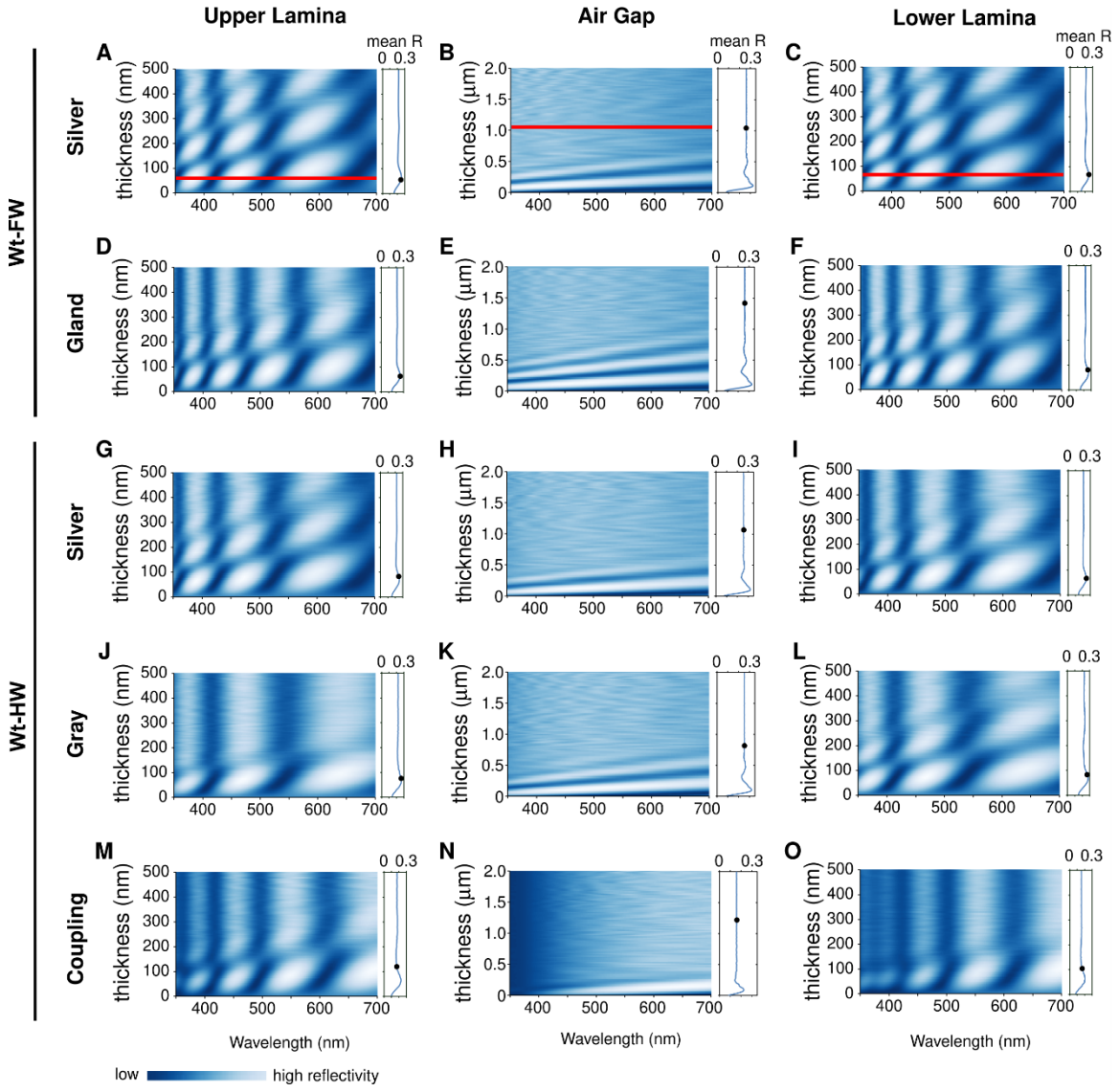

Supplementary Figure S4: Simulations over the parametric space of the five different wildtype silver scales of *B. anynana* to understand how changing one layer thickness at a time affects broadband color production. Related to Figure 1. Theoretical reflectivities (relative to a specular standard) modeled by systematically changing the layer thickness of upper lamina (first column), air gap (second column) or lower lamina (third column), while keeping the other two parameters constant, are plotted as heatmaps. The heatmaps are top-views of a complex 3-D dataset of 100 spectra extrapolated across the range of thickness values (with wavelength along *x*, thickness along *y* and reflectivity/intensity along *z*), so that the peaks (high intensity) in the spectra are shown in shades of white and dips (low intensity) in navy blue. For reference, the reflection spectra corresponding to the thick red lines in **A**-**C** are as plotted in Fig. S3A (red, blue and black dashed curves). The inset plots on the right show the mean broadband reflectivity, *R*, averaged over the entire wavelength range at each thickness value and the black dot denotes the corresponding measured layer thickness for that specific scale type (see Fig 1I, and Supplementary Table S5 – source data). *R* is largely constant across the thickness range

but shows a small peak at the lower end of the range. The observed lower and upper lamina thickness for all silver scales except coupling seem to lie at or very close to this peak, *i.e.*, they seem to be optimized for maximal broadband brightness. The air gap thicknesses are, however, not optimized for maximal brightness (at the lower end of the range), but rather thick enough to ensure the reflectivity is achromatic and broadband (i.e., uniform or flat). Varying only upper (left column) or lower lamina (right columan) thicknesses even upto 500 nm shows that the spectra still remain sinusoidal and chromatic because of the pronounced peaks (strong white areas). Only by varying air gap thickness (middle column), do we obtain nearly uniform broadband reflectivity above a certain thickness threshold (diffused patterns in column B). The coupling scales, which are the least pigmented among any of the silver scale types, are a natural experiment that illustrates the effect of increasing the upper and lower lamina thickness beyond their optimal values. Similar to the effect of the thickened lamina near the ridges (Supp Figs. S3C, and D), the coupling lamina thicknesses, which are above the optimum, reduce the intensity at shorter wavelengths (notice the darker blue color in Figs. S4M-O at these wavelengths), analogous to the effects of short-wavelength absorbing pigments (see Fig 1B‴-F‴).

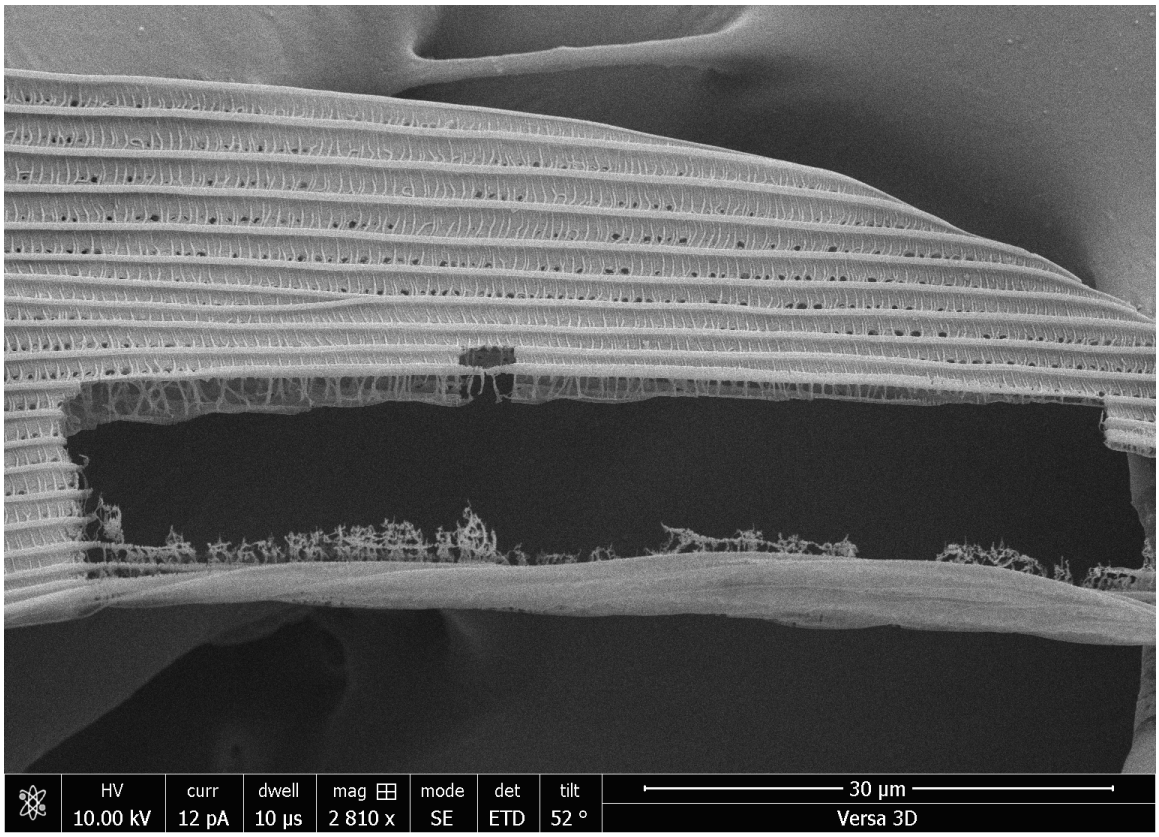

Supplementary Figure S5: Longitudinal cross-section of a wildtype coupling scale of *Bicyclus anynana*. Related to Figure 1. Proximal base of the scale is to the left. The thickness of the lower lamina decreases from the base (left) to the tip (right) of the scale. The hole in the middle corresponds to a region previously milled using the FIB for the thickness measurements.

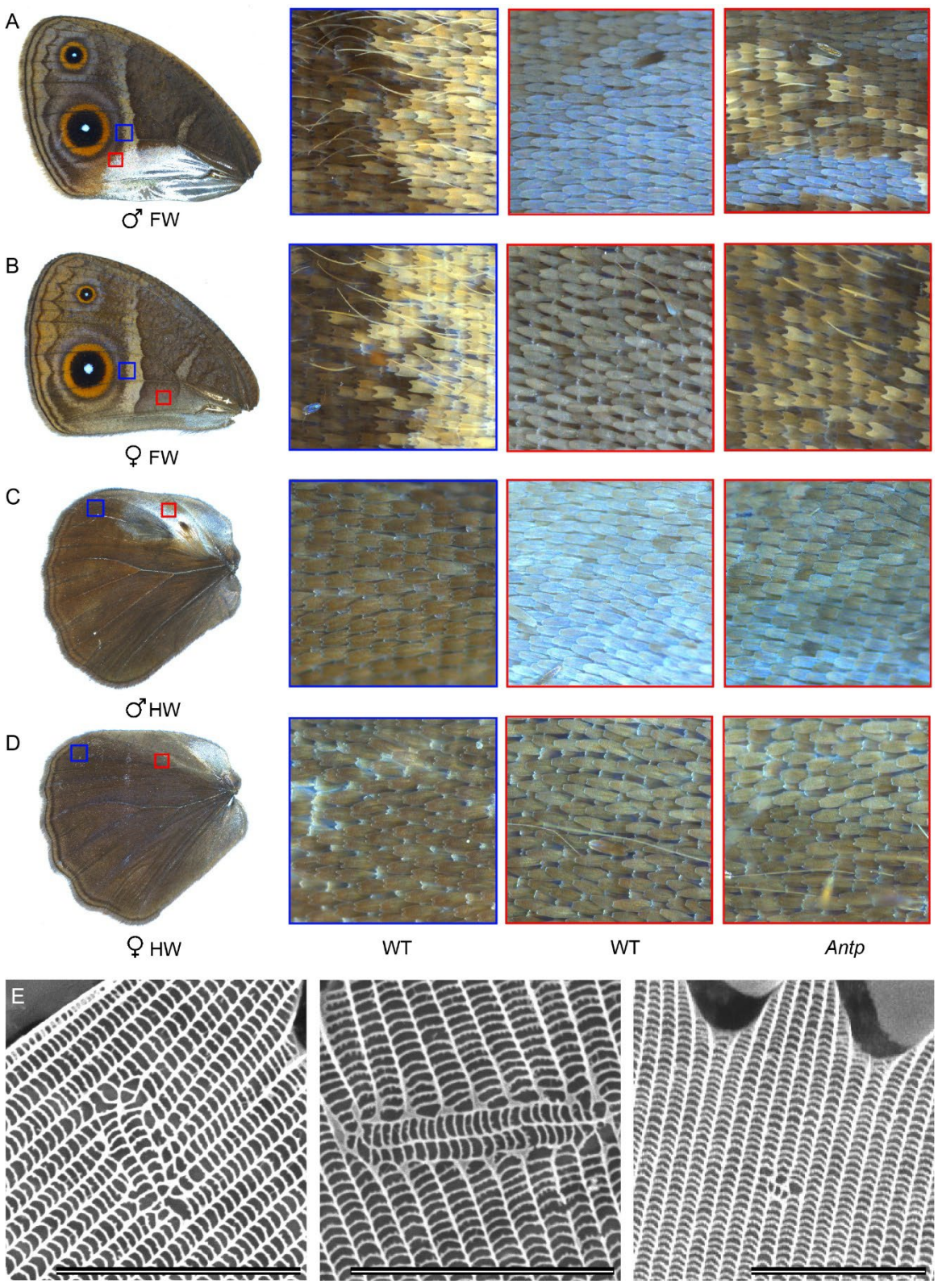

Supplementary Figure S6: Scale shape in the wildtype and *Antp* crispant wings of *Bicyclus anynana* and scale ultrastructure in *Antp* crispants. Related to Figure 2. (A, B) Ventral male and female forewings (C, D) Dorsal male and female hindwings. The colored boxes mark the positions on the wing that were imaged. The blue boxes are the control regions where all scales have a dentate distal margin. The red boxes are the regions on the wings that were affected in

the *Antp* crispants (dentate scales) as compared to the wildtype (rounded scales). (E) SEM images of *Antp* crispant forewing brown scales showing examples of orthogonal ridge and crossrib orientation among the normal ridges and crossribs. All scales are from one individual. Scale bars are 20 μm.

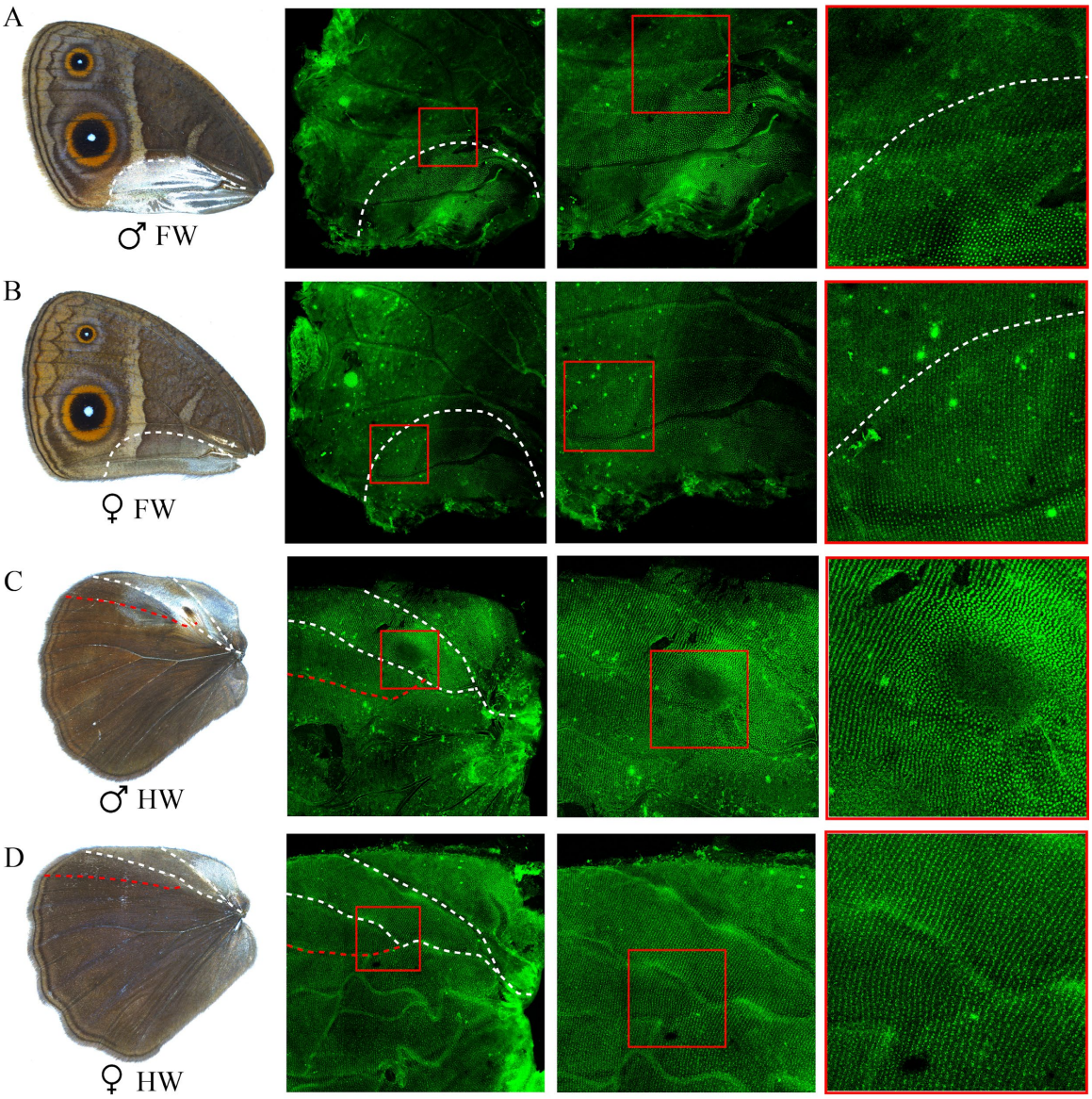

Supplementary Figure S7: Immunostainings of *Bicyclus anynana* male and female 24-hour pupal wing discs with anti-Antp antibody. Related to Figure 2. Stainings are shown for (A, B) male and female ventral forewings and (C, D) male and female dorsal hindwings. The white dotted line on the forewings indicates homologous areas on the posterior wings of both sexes where Antp protein is present. The white and red dotted lines on the hindwings highlight homologous veins. The boxed regions are magnified in the last column. Images are the best, illustrative images.

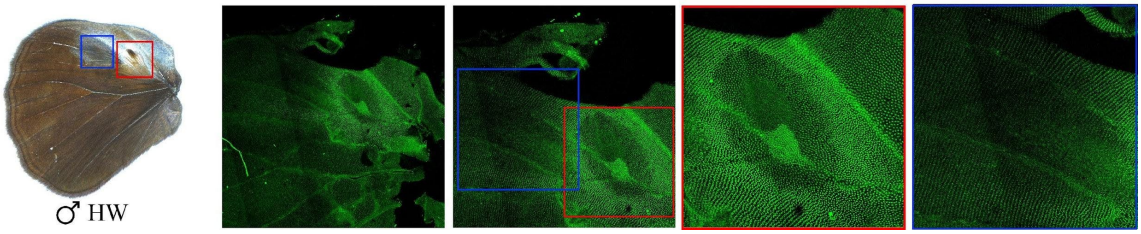

Supplementary Figure S8: Immunostaining of *Bicyclus anynana* male 48-hour pupal hindwing with anti-Antp antibody. Related to Figure 2. The red and the blue regions highlight the silver scale region and grey-silver scale region of the hindwings respectively. Antp is present at high levels in the silver scales surrounding the androconia with absence in the brownish-yellow scales in the androconial patch (red box). Low levels of Antp are seen in the grey-silver scale region (blue box).

Supplementary Table S1: Outcomes of the LME tests comparing area of open upper lamina among wildtype silver scales and between wildtype and crispant scales. Related to Figures 1, 2, 3 and 4

Factor	numDF	denDF	F-value	P-value
Fig 1: Area of open upper lamina in wildtype silver scales				
Crispant	4	46	17.79	**<0.0001**
Fig 2: Area of open upper lamina in *Antp* and *dsx* forewing crispant brown scales compared to wildtype silver scales				
Crispant	2	23	709.7	**<0.0001**
Fig 3: Area of open upper lamina in *apA*, *dsx* and *optix* hindwing crispant brown scales compared to wildtype silver scales				
Crispant	7	82	119.09	**<0.0001**
Fig 4: Area of open upper lamina in *apA* and *Ubx* ectopic silver scales compared to control brown scales				
Crispant	4	37	489.82	**<0.0001**

Supplementary Table S2: Estimates, 95% CI and adjusted P-values for the multiple comparisons of area of open upper lamina among different scale types obtained from Tukey post-hoc tests. Related to Figures 1, 2, 3 and 4

Comparison	Estimate (%)	Std. error	z-value	Pr(>|z|)	95% CI
Fig 1: Comparisons of area of open upper lamina among wildtype silver scales					
FW silver – FW gland == 0	-0.29	0.09	-3.29	**0.01**	-0.53 to -0.06
HW grey-silver – HW coupling == 0	3.07	1.47	2.09	0.361	-0.74 to 6.89
HW silver – HW grey-silver ==0	-4.69	1.45	-3.23	**0.01**	-8.48 to -0.91
Fig 2: Area of open upper lamina of *Antp* and *dsx* forewing crispant brown scales in comparison to wildtype silver scales					
WT silver – *Antp* brown == *0*	-41.15	1.2	-34.41	**<2e-16**	-43.92 to -38.38
WT silver – *dsx* brown == 0	-24.27	1.58	-15.34	**<2e-16**	-27.93 to -20.60
dsx brown – *Antp* brown == 0	-16.88	1.98	-8.51	**<2e-16**	-21.47 to -12.29
Fig 3: Area of open upper lamina of *apA*, *dsx* and *optix* hindwing crispant brown scales in comparison to wildtype silver scales					
optix brown – WT coupling silver == 0	26.75	1.8	14.88	**< 2e-16**	21.44 to 32.06
HW silver region					

WT silver – *apA* brown == 0	-31.57	2.09	-15.1	**< 2e-16**	-37.74 to -25.4
WT silver – *dsx* brown == 0	-27.9	2.49	-11.20	**< 2e-16**	-35.23 to -20.54
HW grey-silver region					
WT grey-silver – *apA* brown == 0	-25.67	2.92	-8.80	**< 2e-16**	-34.28 to -17.06
WT grey-silver – *dsx* brown == 0	-23.70	2.36	-10.02	**< 2e-16**	-30.69 to -16.72
Fig 4: Area of open upper lamina of *apA* and *Ubx* ectopic silver scales compared to control brown scales					
apA silver – control brown == 0	-40.72	2.52	-16.19	**< 2e-16**	-47.28 to -34.17
apA gland – control brown == 0	-33.48	2.88	-11.61	**< 2e-16**	-40.997 to -25.96
apA silver – *apA* gland == 0	-7.25	1.42	-5.12	**3.13e-06**	-10.94 to -3.56
Ubx silver – control brown == 0	-39.69	0.97	-40.85	**< 2e-16**	-42.22 to -37.16

Supplementary Table S3: Outcomes of the LME tests comparing lamina thicknesses among wildtype silver scales and between wildtype and crispant scales. Related to Figures 1, 2, 3 and 4

Factor	numDF	denDF	F-value	P-value
Fig 1: Lamina thickness of wildtype silver scales				
Crispant	9	537	47.82	**<0.0001**
Fig 2: Lamina thickness of *Antp* and *dsx* forewing crispant brown scales in comparison to wildtype silver scales				
Crispant	2	225	203.87	**<0.0001**
Fig 3: Lamina thickness of *apA*, *dsx* and *optix* hindwing crispant brown scales in comparison to wildtype silver scales				
Crispant	7	590	87.41	**<0.0001**
Fig 4: Lamina thickness of *apA* and *Ubx* ectopic silver scales in comparison to control brown scales				
Crispant	7	581	201.68	**<0.0001**

Supplementary Table S4: Estimates, 95% CI and adjusted P-values for the multiple comparisons between lamina thicknesses obtained from Tukey post-hoc tests. Related to Figures 1, 2, 3 and 4

Comparison	Estimate (nm)	Std. error	z-value	Pr(>|z|)	95% CI
Fig 1: Lamina thickness comparisons of wildtype silver scales					
FW silver LL – FW silver UL == 0	10.56	2.38	4.44	**0.0004**	3.10 to 18.01
FW gland LL – FW gland UL == 0	15.49	2.35	6.60	**1.85e-09**	8.14 to 22.85
HW silver LL – HW silver UL == 0	-14.59	3.48	-4.19	**0.0012**	-25.48 to -3.69
HW grey LL – HW grey UL == 0	6.24	3.49	1.79	1.00	-4.71 to 17.18
HW coupling LL – HW coupling UL == 0	-22.39	4.71	-4.75	**9.02e-05**	-37.14 to -7.63
Fig 2: Lamina thickness of *Antp* and *dsx* forewing crispant brown scales in comparison to wildtype silver scales					
Dsx brown LL - *Antp* brown LL == 0	-36.27	2.64	-13.75	**<2e-16**	-42.45 to -30.1
WT FW silver LL – *Antp* brown LL == 0	-61.3	3.11	-19.69	**<2e-16**	-68.58 to -54.01
WT FW silver LL – *Dsx* brown LL == 0	-25.03	2.9	-8.63	**<2e-16**	-31.81 to -18.24
Fig 3: Lamina thickness of *apA*, *dsx* and *optix* hindwing crispant brown scales in comparison to wildtype silver scales					
optix brown LL – WT coupling silver LL == 0	-7.67	4.40	-1.74	1.00	-20.93 to 5.59
HW silver region					
apA brown LL – WT silver LL == 0	36.42	2.66	13.70	**< 2e-16**	28.42 to 44.42
dsx brown LL – WT silver LL == 0	33.4	3.024	11.04	**< 2e-16**	24.29 to 42.50
HW grey-silver region					
apA brown LL – WT grey-silver LL == 0	42.92	2.92	14.72	**< 2e-16**	34.14 to 51.7
dsx brown LL – WT grey-silver LL == 0	10.02	3.04	3.30	**0.027**	0.88 to 19.16
Fig 4: Lamina thickness comparisons of *apA* and *Ubx* ectopic silver scales and control					

apA silver LL – control brown LL == 0	-59.63	3.14	-19.02	**< 2e-16**	-69.05 to -50.21
apA gland LL – control brown LL == 0	-55.13	3.02	-18.26	**< 2e-16**	-64.20 to -46.06
Ubx silver LL – control brown LL == 0	-62.70	2.86	-21.93	**< 2e-16**	-71.29 to -54.11
apA silver LL – *apA* silver UL == 0	7.2	1.90	3.78	**0.0043**	1.48 to 12.91
apA gland LL – *apA* gland UL == 0	10.90	1.68	6.49	**2.42e-09**	5.85 to 15.95
Ubx silver LL – *Ubx* silver UL == 0	15.65	2.74	5.72	**3.00e-07**	7.42 to 23.86

Supplementary Table S6: List of gRNA sequences used to generate the crispants in this study, complied from previous publications. The regions targeted by each gRNA are mentioned. Related to STAR Methods.

Gene	gRNA sequence (5' -> 3')	Region targeted	Reference
apterous A *(apA)* Guide 1	GAAATTAATACGACTCACTATAGGAGCTGGTGATGCTTGAAGCGTTTTAGAGCTAGAAATAGC	Homeodomain	Prakash and Monteiro 2018, Proc R Soc B
apterous A (apA) Guide 2	GAAATTAATACGACTCACTATAGGAGAAACAGTGCACATGAAACACGTTTTAGAGCTAGAAATAGC	LIM domain	
Ultrabithorax *(Ubx)* Guide 1	GAAATTAATACGACTCACTATAGGCTGCCACGGAGGCGTCGTGTTTTAGAGCTAGAAATAGC	Exon 1	Matsuoka and Monteiro 2021, Genetics
Ultrabithorax (Ubx) Guide 1	GAAATTAATACGACTCACTATAGGCGTGCACCAGGGCGGTGGGTTTTAGAGCTAGAAATAGC	Exon 1	
doublesex (dsx)	GAAATTAATACGACTCACTATAGGTACTTGCAGTACCGCTTGGTTTTAGAGCTAGAAATAGC	Common exon 1 for both isoforms, *dsxM* and *dsxF*	Prakash and Monteiro 2020, MBE

Antennapedia (Antp) Guide 1	GAAATTAATACGACTCACTATAGGGTAAGGCATGCCAGGGGCGTTTTAGAGCTAGAAATAGC	Exon 1	Matsuoka and Monteiro 2021, Genetics
Antennapedia (Antp) Guide 2	GAAATTAATACGACTCACTATAGCGACCAGCAGCTCAGGCCCGTTTTAGAGCTAGAAATAGC	Exon 1	
optix Guide 1	GAAATTAATACGACTCACTATAGGGGCTTCGCAGCGCTCCAGCTGTTTTAGAGCTAGAAATAGC	SIX1_SD domain	Das Banerjee, Seah and Monteiro, Biorxiv
optix Guide 2	GAAATTAATACGACTCACTATAGGTTCTTCGTCGGGTTCGGGTAGTTTTAGAGCTAGAAATAGC	Homeodomain	